

This manuscript is a non-peer reviewed preprint and has been submitted for publication in Remote Sensing of Environment. Please note that subsequent versions of this manuscript may have different content. Please feel free to contact any of the authors; we welcome feedback.

# **High Accuracy Estimation and Validation of InSAR-derived Surface Displacements at Temperate Raised Peatlands**

Alexis Hrysiewicz<sup>1,2</sup>, Jennifer Williamson<sup>3</sup>, Chris D. Evans<sup>3</sup>, A. Jonay Jovani-Sancho<sup>3,4</sup>, Nathan Callaghan<sup>3</sup>, Justin Lyons<sup>5</sup>, Jake White<sup>5</sup>, Joanna Kowalska<sup>5</sup>, Nina Menichino<sup>5</sup> and Eoghan P. Holohan<sup>1,2</sup>

<sup>1</sup>SFI Research Centre in Applied Geosciences (iCRAG), University College Dublin, Dublin, Ireland

<sup>2</sup>UCD School of Earth Sciences, University College Dublin, Dublin, Ireland

<sup>3</sup>UK Centre for Ecology & Hydrology, Bangor, United Kingdom

<sup>4</sup>School of Biosciences, University of Nottingham, Loughborough, United Kingdom

<sup>5</sup>Natural Resources Wales, United Kingdom

**Corresponding author: Alexis Hrysiewicz ([alexis.hrysiewicz@ucd.ie](mailto:alexis.hrysiewicz@ucd.ie))**

**This manuscript is a non-peer reviewed preprint and has been submitted for publication in Remote Sensing of Environment. Please note that subsequent versions of this manuscript may have different content.**

**Please feel free to contact any of the authors; we welcome feedback.**



# **High Accuracy Estimation and Validation of InSAR-derived Surface Displacements at Temperate Raised Peatlands**

Alexis Hrysiewicz<sup>1,2</sup>, Jennifer Williamson<sup>3</sup>, Chris D. Evans<sup>3</sup>, A. Jonay Jovani-Sancho<sup>3,4</sup>, Nathan Callaghan<sup>3</sup>, Justin Lyons<sup>5</sup>, Jake White<sup>5</sup>, Joanna Kowalska<sup>5</sup>, Nina Menichino<sup>5</sup> and Eoghan P. Holohan<sup>1,2</sup>

<sup>1</sup>SFI Research Centre in Applied Geosciences (iCRAG), University College Dublin, Dublin, Ireland

<sup>2</sup>UCD School of Earth Sciences, University College Dublin, Dublin, Ireland

<sup>3</sup>UK Centre for Ecology & Hydrology, Bangor, United Kingdom

<sup>4</sup>School of Biosciences, University of Nottingham, Loughborough, United Kingdom

<sup>5</sup>Natural Resources Wales, United Kingdom

Corresponding author: Alexis Hrysiewicz ([alexis.hrysiewicz@ucd.ie](mailto:alexis.hrysiewicz@ucd.ie))

## **Highlights**

- New InSAR method to retrieve accurate surface motions at temperate peatlands
- InSAR-derived motions validated on raised peatlands with novel camera-based sensors
- Validation of InSAR data to mm-level accuracy at equivalent temporal resolution
- Annual InSAR-derived bog breathing linked to changes in shallow groundwater levels
- Method has potential for monitoring and verification of peatland restoration

## Abstract

Peatland surface motion derived from satellite-based Interferometry of Synthetic Aperture Radar (InSAR) is potentially a proxy for groundwater level variations and greenhouse gas emissions from peat soils. Ground validation of these motions at equivalent temporal resolution and accuracy has proven problematic because of limitations of traditional surveying methods. Since 2019, peat surface motion has been measured *in-situ* using novel camera-based instrumentation at two temperate raised bogs, Cors Fochno and Cors Caron, Wales, United Kingdom. The cameras provide continuous measurements at sub-millimetre precision and sub-daily temporal resolution. From these and Sentinel-1 acquisitions spanning mid-2015 to early-2023, we demonstrate that accurate InSAR-derived peat surface motion can be derived using a combination of interferometric networks comprising long and short temporal baselines. The InSAR time series data closely match the *in-situ* data at both bogs, in particular the annual peat surface oscillations. Pearson's values for the correlation of *in-situ* and InSAR displacements are 0.8-0.9, and 76 % of differences are  $< \pm 5$  mm (93 %  $< \pm 10$  mm). Larger differences mainly occur during drought periods. Multi-annual displacement velocities based on InSAR indicate long-term subsidence of the Cors Caron surface (max.  $-7$  mm $\cdot$ yr $^{-1}$ ) while that of Cors Fochno exhibits subsidence at the centre and uplift at the margins ( $-9$  mm $\cdot$ yr $^{-1}$  to  $+5$  mm $\cdot$ yr $^{-1}$ ). These long-term peat surface subsidence rates correlate well with peat dome elevation and peat thickness. In addition, the annual oscillations in surface motion are synchronous with or lag slightly behind groundwater level changes. A coarse ratio of 1:20 to 1:10 is observed between annual changes in groundwater levels and peat surface displacements. Satellite-based InSAR can thus enable accurate monitoring of hydrologically driven surface motions of temperate raised peatlands.

# 1. Introduction

Peat soils store an estimated 20-30 % of global soil carbon ([Drösler et al., 2008](#); [Gorham, 1991](#); [Köchy et al., 2015](#); [Renou-Wilson et al., 2019](#); [Yu et al., 2010](#)). As a result of drainage for agriculture and plantation forestry, fires, and other forms of habitat degradation, peatlands are estimated to contribute between 2 % and 5 % of global GHG emissions (e.g., [Joosten et al., 2016](#); [Smith et al., 2014](#)). The large uncertainty range reflects a lack of knowledge regarding both the extent, and the impact on emissions, of peatland modification. Reducing this knowledge gap has become a priority in the current scientific research context and governmental policy guidelines, with the goal to protect peatlands and restore carbon sink capacity to partially mitigate worldwide global warming ([Hiraishi et al., 2014](#); [Leifeld & Menichetti, 2018](#); [Letts et al., 2000](#)). In addition, the preservation and restoration of peatlands are critical for preserving their unique flora and fauna in support of the nature crisis which is intrinsically linked to ecosystem resilience ([Renou-Wilson et al., 2019](#)).

Traditionally, peatland monitoring has relied primarily on in-situ measurements at local scale to estimate and to upscale various ecohydrological parameters: i.e., groundwater level changes, soil moisture changes, peat temperature and peat thickness. Extension of such monitoring of peatlands to regional, national, or global scales is a challenge. Indeed, approximately 3 % of the world land area, amounting to 4.23 million km<sup>2</sup>, is peat soil ([Xu et al., 2018](#)). This rises to 12 % of the United Kingdom (UK) – c. 29,500 out of 241,930 km<sup>2</sup> ([Evans et al., 2017](#); [Smyth et al., 2017](#)). Consequently, remote sensing methods over peatlands have developed to estimate key eco-hydrological parameters, such as variations in soil moisture (e.g., [Asmuß et al., 2018](#); [Balenzano et al., 2021](#); [Balenzano et al., 2012](#); [Bechtold et al., 2018](#); [Connolly & Holden, 2009](#); [Connolly & Holden, 2017](#); [Kim et al., 2017](#); [Lees et al., 2018](#); [Millard & Richardson, 2018](#); [Millard et al., 2018](#); [Paloscia et al., 2013](#); [Peng et al., 2021](#);

[Takada et al., 2009](#); [Wagner et al., 2013](#); [Xu et al., 2018](#)), and groundwater level, with medium spatial resolution (~1 km), large spatial coverage (regional and country scales) and relatively low cost.

Ground surface motion in peatlands, or “bog breathing”, has long been linked with ecological conditions, meteorological changes and/or hydrogeological variations (e.g., [Evans, Peacock, et al., 2021](#); [Hooijer et al., 2012](#); [Howie & Hebda, 2018](#); [Morton & Heinemeyer, 2019](#); [Regan et al., 2019](#); [Van den Akker et al., 2012](#)). Moreover, empirical models have been proposed to relate in-situ subsidence measurements, groundwater level changes and carbon loss via GHG emissions ([Hooijer et al., 2010](#); [Hooijer et al., 2012](#); [Hooijer et al., 2014](#)). Obtaining representative in-situ measurements of peat surface motions is complicated, however, by the mechanical properties of peat and by the costs and/or limitations of traditional surveying techniques and equipment.

Most past efforts to measure peatland surface motions in-situ have focussed on the use of subsidence poles or precise levelling surveys. These have measured the elevations of ground on the peatland either directly (e.g., [Howie & Hebda, 2018](#); [Tampuu, 2022](#); [Tampuu et al., 2022](#)) or indirectly (e.g., [Bradley et al., 2022](#); [Marshall et al., 2022](#)). These survey methods offer the advantage of giving cm-scale to mm-scale precision but have the disadvantage of being highly discontinuous in time (measurements typically monthly to yearly) and cost-intensive in terms of equipment, fieldwork, and staff time. Other efforts have involved the installation of continuous Global Navigation Satellite System (cGNSS) stations ([Reeve et al., 2013](#)). These have the advantage of providing more continuous measurements in time (hourly to daily). However, cGNSS is relatively inaccurate to vertical motions that predominate at peatlands, such that the precision of measurement is on the order of several cm. In addition, secure installation, and maintenance over many years of such expensive electronic equipment in a water-logged highly acidic environment is challenging. Recently [Evans, Callaghan, et al. \(2021\)](#) developed an *in-situ* method to continuously monitor peat surface motion

based on a vertical pole fixed into the substrate below the peat and a time lapse camera that is able to move vertically with the peat surface. This method bypasses the limitations of previous techniques in term of accuracy, cost and temporal sampling.

Recently, satellite-based Interferometry of Synthetic Aperture Radar (InSAR) has made it possible to estimate ground surface motion at large scale, high spatial resolution, and low cost by using open-data such as Sentinel-1 data (C band). A key advantage of radar remote sensing is the ability to provide estimates with a consistent temporal resolution because observations are not hindered by cloud cover: i.e., a 6/12-day temporal resolution can be expected with Sentinel-1 satellites. Application of InSAR to measuring peatland surface motion has been undertaken for both temperate (e.g., [Alshammari et al., 2020](#); [Alshammari et al., 2018](#); [Fiaschi et al., 2019](#)) and tropical peatlands ([Hoyt et al., 2020](#); [Zhou, 2013](#); [Zhou et al., 2016](#)). However, recent ground validation efforts show that existing approaches to InSAR computations on peatlands apparently fail to capture with accuracy both the longer-term trend of peat surface motion and the shorter-term variations in surface motion superimposed on that trend ([Marshall et al., 2022](#); [Tampuu, 2022](#); [Tampuu et al., 2022](#)). Consequently, improved application of InSAR to mapping peatland surface motion requires refinement of the processing techniques, but such refinement must go hand-in-hand with validation through an *in-situ* technique of compatible precision and temporal resolution.

In this study, we compare surface motion derived from InSAR at two temperate raised bogs in Wales, United Kingdom (UK) to surface motion derived from the novel high-precision (sub-millimetre), high-frequency (sub-daily) and low-cost approach based on digital cameras ([Evans, Callaghan, et al., 2021](#)). After presenting the two peatlands, we outline the methodologies used for InSAR estimation and *in-situ* measurements. We then present the InSAR-derived peat surface motion velocities, and compare the time series of vertical peat motions with the *in-situ* motion. Finally, we investigate the

relationships between peat surface motion, peat thickness and groundwater level change. Our results provide a robust, high-precision and high-frequency ground validation of InSAR-derived motion for peatlands. This work also provides the basis for greater confidence in future use of InSAR-derived observations for decision-makers in peatland management.

## 2. Study sites

### 2.1. Geological context and Management History

Cors Fochno and Cors Caron are two temperate raised peatlands located in Wales (UK) (**Figure 1a**). Cors Fochno is located less than 1 km from the coast at elevations of <10 m.a.s.l (see **Figure 1a**), whereas Cors Caron lies about 17 km inland at elevations of ~160-170 m.a.s.l. Cors Fochno comprises one continuous peatland area (see **Figure 1b**), whereas Cors Caron is divided into three sub-areas (or units): west, north-east, and south (see **1c**). Both areas are underlain by Silurian mudstones ([Cave et al., 1984](#); [Davies et al., 1994](#)) and underwent glacial erosion and sedimentation in Quaternary period. From borehole data, Cors Fochno peat lies directly on estuarine clays ([Godwin, 1943](#)).

Both sites have been affected by historic and current land-use challenges, including drainage of the bog periphery or agriculture and peat cutting. Currently, both bogs therefore are protected by national and international conservation directives and have been subject to restoration works in recent decades. Nationally, Cors Fochno and Cors Caron are Special Areas of Conservation (SAC) (site codes: UK0014791 and UK0014790, respectively). Internationally, both were NATURA 2000 sites (depreciated) and are currently sites for the EU LIFE programme, while Cors Fochno is in the Dyfi UNESCO Biosphere area.

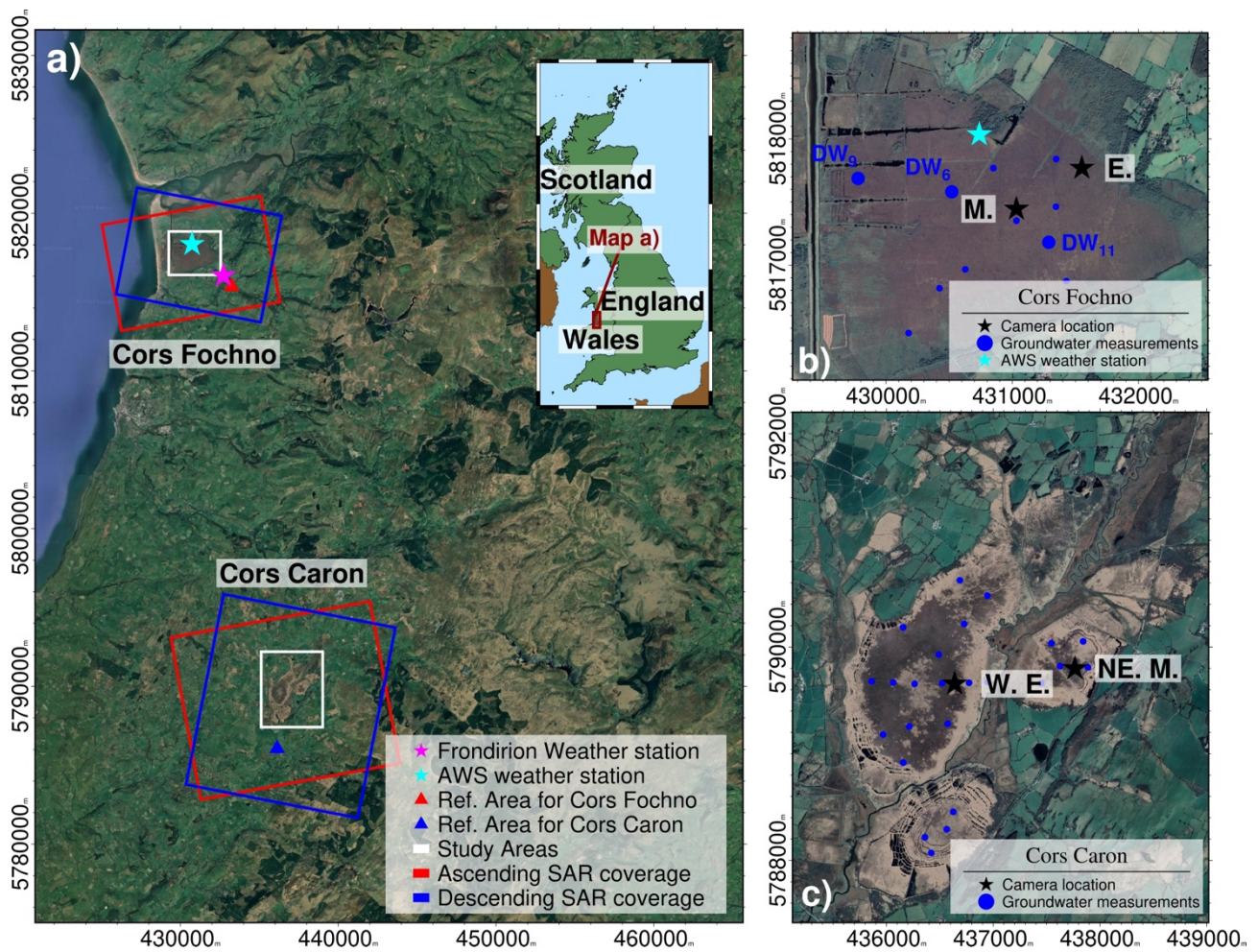


**Figure 1:** The peatland study sites. **a)** Natural colour satellite image with locations of the studied peatlands, the SAR data coverage and the InSAR reference points. The inset map shows the study area location within Great Britain. **b)** Natural colour satellite image of Cors Fochno site from Google Earth<sup>®</sup>: September 2019. **c)** Natural colour satellite image of Cors Caron site from Google Earth<sup>®</sup>: April 2021. Camera locations are shown as black stars in each panel. At Cors Fochno, the camera stations are named: M.: Middle, E.: Edge. At Cors Caron, the camera stations are named: W. E.: West Edge and NE. M.: Northeast Middle. Groundwater level measurement stations are shown as blue dots in each panel. On Cors Fochno, the bigger labelled blue dots represent the stations discussed in the main text. The grids are given in 30U UTM meters.

The hydrology of Cors Fochno has been influenced since the mid-17<sup>th</sup> century by drainage for two purposes: peat cutting and creation of grazing land. Of the 652 ha of the Cors Fochno SAC, 200 ha is

classified as primary (uncut) but even this is dissected by some significant large ditches as well as numerous small ones. Of the remaining 452 ha, a large proportion has been cut domestically for peat and some areas have also been managed and drained for pasture. In the past, the entire periphery of the SAC has an over-deepened drainage network of approximately 14 km. Internally, there are over 23 km of large to medium ditches within the SAC. Nearly all of these have been dammed as part of hydrological restoration works, mainly over the last 30 years. The period 2000 – 2016 saw extensive blocking of cuttings, mainly on the south of the site and to a lesser degree on the eastern part of the dome. Between 2016 to 2022, low-profile contour bunding has been used to improve the sites hydrology. Most of this work was carried out as part of the LIFE Welsh Raised Bog Project, with the construction of an extensive network of contour bunds.

Cors Caron has been subject to several restoration attempts via rewetting since the 1990's, when large peat dams were built initially around the periphery of all three bog domes to hold water on them. In the 2000's, smaller dams were built within the peat cutaway areas up to the peat cliff, and observed surface cracks and ditches were blocked by using plastic piling. Since 2020, low-elevation contour bunds have been installed on the raised domes themselves.

## 2.2. Meteorological context

**Figure 2** gives an overview of meteorological data obtained from HadUK-Grid ([Hollis et al., 2019](#)) and local stations for Cors Fochno: Frondirion and AWS stations (see **Figure 1a**). HadUK-Grid is a kilometre-scale grid of weather data interpolated from the in-situ stations of the UK Meteorological Office (MET). Frondirion station is outside the Cors Fochno area and measures the daily rain precipitations since 1981. AWS station (for Automatic Weather station) is located on Cors Fochno and measures several weather parameters (i.e., daily rainfall, daily air temperature). However, there are many observation gaps with this station.

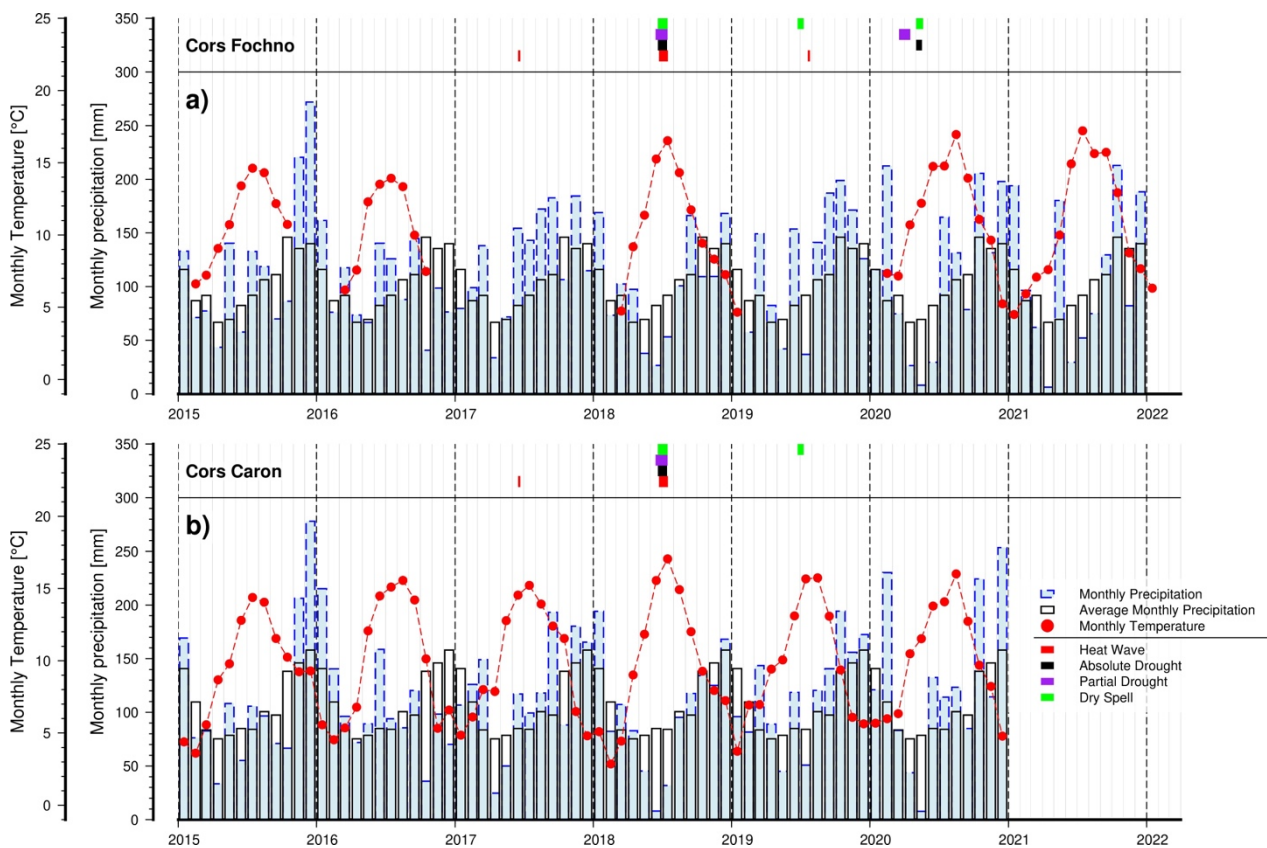


**Figure 2** Weather data from HadUK-Grid and local stations on Cors Fochno in **a)** and Cors Caron in **b)**. For Cors Fochno, the light blue bars are the total monthly rain precipitation from data measured by Frondirion station, whereas the unfilled bars show the average monthly precipitation over the period 1981-2021. The red dots represent the monthly temperatures measured by AWS station. For Cors Caron, the same parameters are computed from the HadUK-Grid data. The drought periods are given at the top of both sub-figures following the UK/IE classification and the HadUK-Grid data.

According to **Figure 2**, average precipitation is 1100-1400 mm·yr<sup>-1</sup> and average annual air temperatures are 6-7 °C for both peatlands. Indeed, the weather varies slightly over the two peatlands as the distance between Cors Fochno and Cors Caron is about 30 km. The climate on Cors Fochno is slightly drier than Cors Caron. The seasonal oscillations in rainfall and temperature (with well-delineated summer and winter periods) are characteristic of a temperate climate. As illustrated at the top of **Figure 2**, there are 4 observed drought periods as per the MET classification: (1) summer 2017,

affected by a short heat wave (for Cors Fochno and Cors Caron); (2) summer 2018, affected by a long-time absolute drought, relative drought, dry spell and heat wave (for Cors Fochno and Cors Caron); (3) summer 2019: affected by a dry spell (for Cors Fochno and Cors Caron) and a heat wave (for Cors Fochno); (4) summer 2020: affected by the three types (absolute, relative, and dry spell) of droughts (for Cors Fochno).

### **3. Datasets and Methods**

#### **3.1. InSAR estimation of peat surface displacements**

##### 3.1.1. Space-based Radar Interferometry for ground surface displacements

Interferometry of Synthetic Aperture Radar (InSAR) is an active remote sensing approach for estimating ground surface displacement from radar data ([Burgmann et al., 2000](#); [Massonnet & Feigl, 1998](#)). The basic principle of InSAR is that a change in the phase of a backscattered signal between two SAR image acquisitions can be directly related to a change in the distance from the radar antenna to ground surface targets (or scatterers). Thus the phase values at each respective pixel within two co-registered SAR images that were acquired on different dates are subtracted to produce an image termed an interferogram. The quality of InSAR is directly controlled by the phase stability – termed InSAR coherence – between the two SAR acquisitions ([Zebker & Villasenor, 1992](#)).

In reality, the differential phase values in the interferogram pixels are not only proportional to the ground surface motions but are also affected by other sources of phase change, such as: orbit inaccuracy, topographic relief, atmospheric delays, and noise ([Massonnet & Feigl, 1998](#)). While orbital and topographic phase corrections are readily achieved, atmospheric phase delay presents a more difficult component to remove from an interferogram. Atmospheric effects can be non-negligible if ground motions between acquisitions are subtle (sub-centimetre). Such effects can be

especially problematic in temperate or humid climates with significant variation of atmospheric moisture in space and time.

Stacking of multiple interferograms from SAR images acquired over time not only enables a timeseries of surface displacement to be obtained at each pixel but also minimises other sources of phase change, especially those related to atmospheric delays. Several approaches have been developed to isolate reliable pixels within the interferogram stack and to obtain their relative displacements as measured along the satellite's line of sight (LOS). These approaches include Permanent Scatterers<sup>®</sup>, Persistent Scatterers, Distributed Scatterers and Small-Baseline Subsets (e.g., [Casu et al., 2006](#); [Ferretti et al., 2011](#); [Ferretti et al., 2001](#); [Hooper, 2008](#)). The temporal evolution of motion obtained from such approaches is given in relation to a reference date and a spatial reference point that is considered stable over the observation period. Displacement rates are estimated by fitting a linear or non-linear trend to the timeseries of observations. The conventional accuracy of InSAR-derived displacement measurements reaches  $\pm 5$  mm for single observations and increases to  $\pm 1$  mm $\cdot$ yr<sup>-1</sup> for displacement rates ([Hanssen, 2001](#)). On conventional target for InSAR with relatively high InSAR coherence, the method has a proven ability to map ground surface displacements on various targets with different surface conditions and displacement rate (cities, volcanoes, earthquakes, landslides, etc.) ([Biggs & Pritchard, 2017](#); [Boncori, 2019](#); [Hanssen, 2001](#); [Hooper et al., 2012](#); [Pinel et al., 2014](#); [Sansosti et al., 2014](#)). Vegetated targets commonly represent more challenging conditions for InSAR methods, however, due to typically low InSAR coherence.

### 3.1.2. Preparation of Sentinel-1 InSAR stack

In this study, we use all available Sentinel-1 A/B data in Interferometric Wide (IW) mode, in both orbital pass directions: ascending (asc., i.e., south to north) and descending (desc., i.e., north to south). The images were acquired on Sentinel-1 Track 30 in ascending orbit and on Sentinel-1 Track 52 in

descending orbit. The combined SAR dataset spans the period from April 2015 to March 2023, i.e., an observation period of more than 7.5 years. With both of the twin Sentinel-1 satellites operational, the temporal resolution is 6 days. The temporal resolution is 12 days when the Sentinel-1B satellite was not available: i.e., before its launch in April 2016 and after its loss in December 2021.

As the Sentinel-1 data, in Single Look Complex (SLC) format, is acquired through a Terrain Observation with Progressive Scans SAR (TOPSAR) imaging mode, a TOPSAR coregistration was performed by using the GAMMA<sup>®</sup> processor ([Wegmüller et al., 2015](#)). For coregistration, reference images are from 2<sup>nd</sup> May 2019 for the ascending dataset and 28<sup>th</sup> May 2019 for the descending stack, according to recent recommendations for selecting the reference dates with respect to application to temperate peatland ([Hrysiewicz et al., 2023](#)). We also use the precise orbits and the SRTM Digital Elevation Model (DEM) ([Farr et al., 2007](#)) to correct for orbital and topographic phase contributions. After obtaining the two co-registered SAR image stacks (ascending and descending) for each studied peatland, each stack of co-registered images was cropped to make four sub-stacks: two (asc. and desc.) for Cors Fochno and two (asc. and desc.) for Cors Caron (see **Figure 1a** for sub-stack coverage).

### 3.1.3. Interferometric network designs

InSAR phase is measured at modulo  $2\pi$  radians: between  $-\pi$  and  $+\pi$  (or 0 to  $2\pi$ ). This is referred to as “wrapped” phase. A crucial step named “unwrapping” allows one to get the cumulative values of phase changes between pixels with respect to a spatial or temporal reference point (e.g., [Chen & Zebker, 2000, 2001](#); [Chen & Zebker, 2002](#)). The unwrapping can be done in 2D (only spatial dimensions) or in 3D (with the temporal dimension) ([Hooper & Zebker, 2007](#)). Importantly, unwrapping methods require continuity of pixels to solve the phase measurement ambiguity – i.e., the uncertainty regarding how many phase cycles of  $2\pi$  radians occur between two pixels of interest

in space or between two phase values for the same pixel in time. Unwrapping is challenging for peatlands, because significant spatial discontinuities within InSAR observations can occur on and around peatlands (see **Figure S1** in Supplementary Materials) depending on factors such as the nature of the peatland vegetation and the processing approach. Phase ambiguities in space and time also can be caused by large amplitude of displacement during dry periods ([Marshall et al., 2022](#); [Tampuu et al., 2022](#)), and unwrapping is further hindered by low InSAR coherence – i.e., phase measurement quality – of lands around the peat soils during these periods ([Hrysiewicz et al., 2023](#)).

The longer-term trend of peat surface motion corresponds to the multi-annual (8-year) rate and direction of surface motion, whereas the shorter-term variations in surface motion corresponds to annual oscillations, or step-like changes, in surface elevation. To estimate multi-annual surface displacement rates correctly, “long-term” interferograms spanning a 1-year period are needed to minimise the potential biases of InSAR phase arising from the interferogram network ([Ansari et al., 2021](#)). Although raised peatlands in good condition can yield 1-year interferograms with moderate to high InSAR coherence (see **Figure S2** in Supplementary Materials) ([Hrysiewicz et al., 2023](#)), interferometric pairs such with such a long temporal baseline can be strongly affected by phase ambiguity ([Marshall et al., 2022](#); [Tampuu et al., 2022](#)). To mitigate the ambiguities, a network of “short-term” interferometric pairs of high InSAR coherence can be used instead. In such a network, each interferogram has a low probability of being affected by phase ambiguity, but multiannual displacement rates are not accurate ([Ansari et al., 2021](#)). Therefore, it is not possible to estimate both displacements and displacement rates accurately by using the same network of interferograms on peatlands.

Knowing these limitations, we designed two types of network to constrain the different components of the peatland surface motions within each of the four interferogram sub-stacks. Consequently, 8

time series of LOS displacements are presented in this study. The two network designs comprise: (1) a “long” temporal baseline network (TBN) ([Ansari et al., 2021](#); [Thollard et al., 2021](#)) to estimate the multiannual velocities of peat surface displacements (**Figure 3a**); and (2) a “short” TBN, in which an image acquired on date D is connected to the successive D+1, D+2 and D+3 images in the set of SLC images (**Figure 3b**), to calculate shorter-term motions. For each stack, both network types contain the interferograms with short temporal baselines, but the “long” TBN additionally contains interferograms of 90 days and 360 days (**Figure 3c,d** and supplementary **Figures S3-S6**).

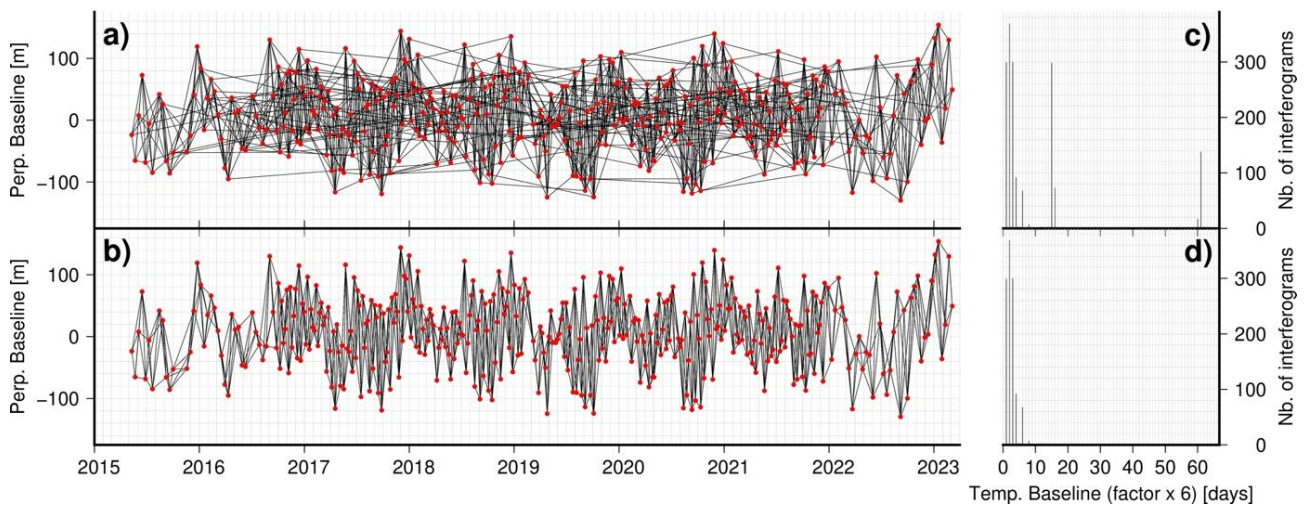


**Figure 3** Example of the two types of network of interferometric pairs used in this study. **a)** Network of interferograms with both long and short temporal baselines. **b)** Network of interferograms with only the short temporal baselines. **c)** Numbers of interferograms versus the temporal baselines for the “long” TBN. **d)** Numbers of interferograms versus the temporal baselines for the “short” TBN. See Supplementary Materials to visualise all of the interferometric networks used for each sub-stack.

### 3.1.4. Time series analysis of peat surface displacements

Extraction of displacements from each sub-stack is performed via the Interferometric Point Target Analysis<sup>®</sup> (IPTA) approach for multi-reference interferogram networks ([Wegmüller et al., 2004](#);

[Werner et al., 2003](#)). The key parameters of the IPTA processing (see **Table S1** in the Supplementary Materials) are identical for all the processing. Only the pixels with high temporal consistency and high coherence were analysed within the IPTA processing networks ([Wegmüller et al., 2004](#); [Werner et al., 2003](#)). Multilooked phases – i.e., phases averaged across several pixels – are estimated by a moving window averaging of phase values across 15 pixels in the range direction and 3 pixels in the azimuth direction. Phases were converted to displacements independently for each peatland and each data sub-stack. The reference point/area for Cors Fochno is in the town of Tal-y-Bont and for Cors Caron it lies in the town of Tregaron (see **Figure 1a**). The same parameters and same reference points are used for all computations on each peatland.

The novelty of the methodological approach presented here is in the combination of results of the long TBN and the short TBN for each sub-stack (**Figure 4**). Firstly, by using a long TBN, we obtain time series of InSAR-derived LOS displacements from which the longer-term multiannual displacement rates should be correctly estimated, but from which the shorter-term displacement variations are underestimated due to phase ambiguities (especially during dry periods). Secondly, the high-coherence pixels identified from the long TBN are also identified as high-coherence pixels from the corresponding short TBN. Therefore, the estimation of displacements on the short TBN within each step of the IPTA processing is made on the point distributions computed from the same step in the processing of the long TBN. Thirdly, we obtain time series of InSAR-derived LOS displacements by using short TBNs, (see **Figure 4**), for which the displacement are correctly estimated but the long-term displacement rates are affected by phase biases ([Ansari et al., 2021](#)). Finally, we create a “combined” dataset of LOS displacements for which the longer-term displacement trend is that estimated from the long TBN and the shorter-term displacement variations are those estimated from the short TBN.

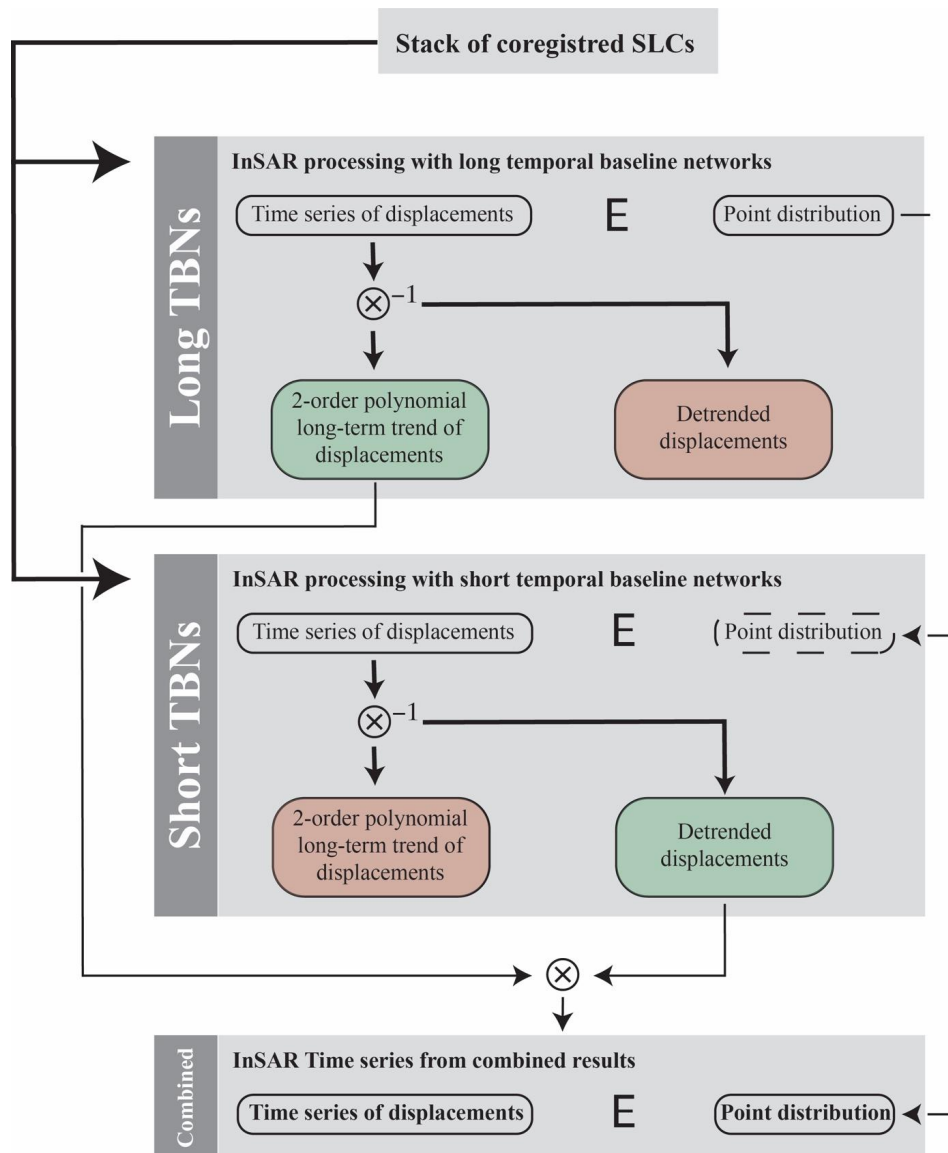


**Figure 4** Workflow for computation of peatland surface displacements. The green results are correctly estimated and the red results are biased.

### 3.1.5. Inversion of vertical and horizontal motions

After obtaining the combined time-series datasets from the ascending and descending tracks, vertical and horizontal (West-East) displacement components are estimated for each peatland by assuming that the South-North component of displacement is negligible (Wright, 2004). Given that the spatial resolution of the multi-looked pixels is  $\sim 40 \times 60$  m, we define a new regular grid (UTM zone 30U) for

each bog at 50 m resolution where only pixels for which we have InSAR points from both datasets (asc. and desc.) are analysed. Then the LOS displacements are spatially interpolated on the grids by using the natural neighbour interpolation method ([Amidror, 2002](#)), while they are temporally interpolated on the dates of the ascending datasets by using a piecewise cubic Hermite polynomial interpolation method ([Fritsch & Carlson, 1980](#); [Kahaner et al., 1989](#)). The vertical and horizontal displacements are estimated by least squares inversion, and the linear displacement rates are recomputed for the vertical and horizontal components. The acquisition dates of the ascending data are thus used as the reference dates for the final timeseries. Uncertainties of displacement on each date are estimated by using the standard deviation values of displacements for the points in the spatial reference areas.

### **3.2. *In-situ* data for peat surface motions, groundwater levels and peat thickness**

The instrument for *in-situ* measurement of peat surface motion comprises a digital camera module mounted on a lightweight platform that is pinned to the peat surface ([Evans, Callaghan, et al., 2021](#)). A 20 mm diameter subsidence pole made of galvanised steel passes through the camera platform and is anchored within the peat body, and ideally within the sub-peat mineral soil: i.e., Cors Fochno peat cameras are anchored in the clay layer (see **Figure 5**). The camera is focussed on a graduated ruler with Aruco (image recognition) markers fixed to the pole. Motion of the camera, and thus of the peatland surface, is with respect to the pole stable in terms of surface motions. The surface displacement is calculated automatically by digital image correlation. The precision of the measurements is sub-mm, and the temporal resolution is daily (for Cors Fochno) or sub-daily (for Cors Caron).

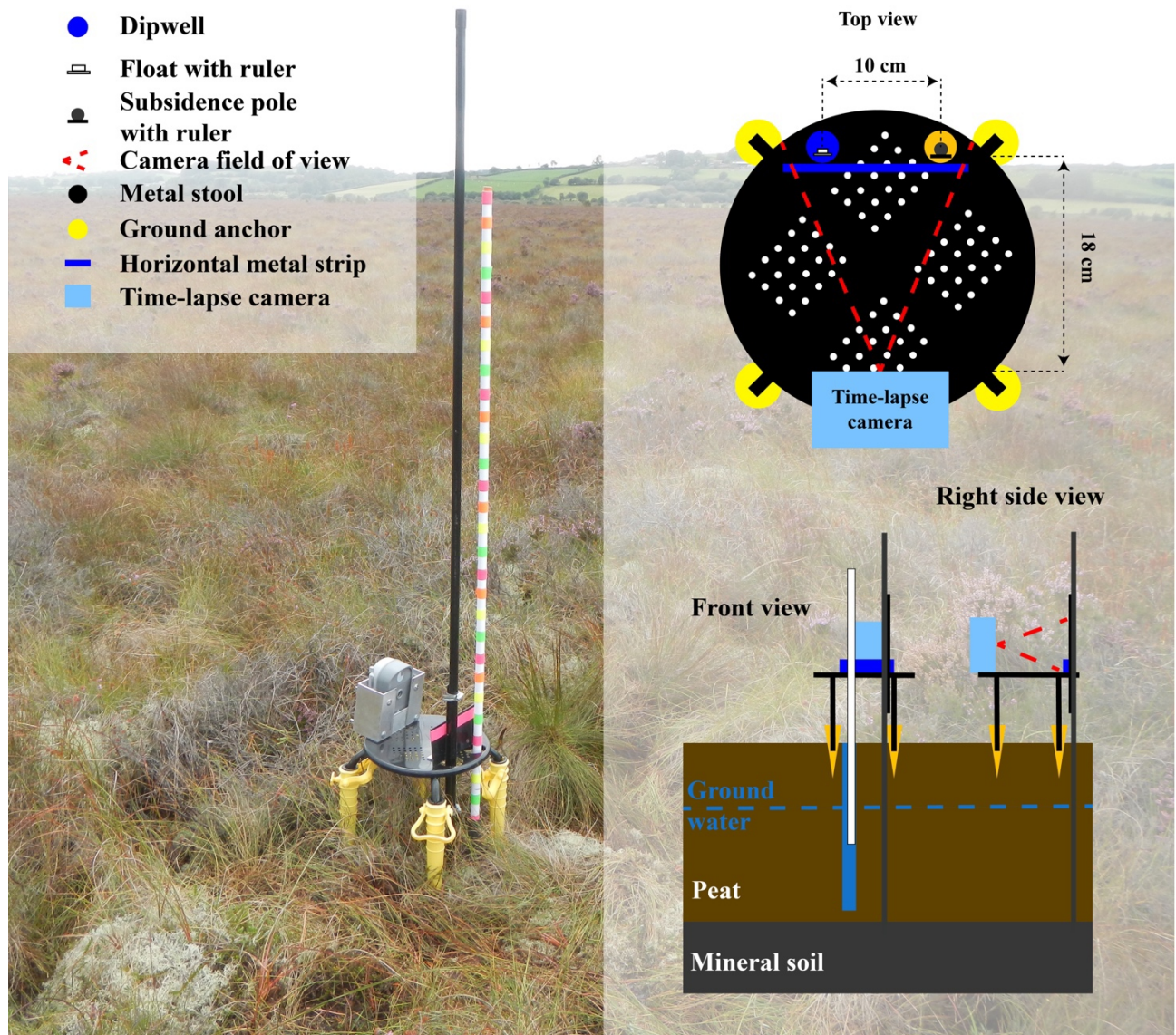


**Figure 5** Picture of a peat camera installed on Cors Fochno, with the associated description. Modified from [\(Evans, Callaghan, et al., 2021\)](#).

The peat-camera measurements cover the period from mid-2019 to late-2022 over both peatlands. Cors Fochno is equipped with two camera stations named Cors Fochno Middle (M.) and Cors Fochno Edge (E.) (**Figure 1b**). Cors Fochno Edge peat camera worked until mid-2021. Cors Caron has two peat camera stations in the areas for which we have InSAR results (**Figure 1c**): the four other stations do not have associated InSAR results or have an observation period less than one year. Their names

are West Edge (W. E.) and Northeast Middle (NE. M.). Regarding the in-situ measurements of displacements, two assumptions are defined in this study: (1) uncertainties associated with peat-camera measurements are negligible compared to InSAR-derived displacements; (2) site visits (i.e., replacing batteries and retrieving data) do not cause any sustained (i.e. step change) displacements on the time series. If not, the step change have been removed in the *in-situ* motion time series.

Cors Fochno is equipped with 11 dip wells, each of 1-m length (36-mm internal diameter) and fixed via a steel pole driven into the basal clay (see **Figure 1b**). Water levels are measured with SOLINST Levelogger 5 and referenced to a standardised peatland surface for each well based on the mean of peatland surface elevation measurements at 33 points within a 2-m radius of each dip well. The purpose of this metric is to take into account in the hydrological assessment the undulating nature of the surface of the bog around each dip well, and to avoid inaccuracies regarding the asynchronous motions between peat surface and tubes. The final observations are given relative to peatland surface. On the three units of Cors Caron (see **Figure 1c**), 21 “floating” dip wells have been installed (i.e., floating along with the peat, and hence providing data relative to the peat surface). Each dip well comprises a tube of 1-m length and contains a SOLINST piezometer, suspended usually around 70-80cm below the peat surface. The dataset of groundwater levels provided from mid-2009 to early 2023.

Peat thickness and surface elevation data for Cors Fochno are derived from ground penetrating radar profiling conducted in 2009. Field inspections indicate that the peat is generally more humified in the bog centre than at the bog edge, especially in the upper 10 cm. Those for Cors Caron are derived from probing in winter 2020/2021. The peat surface elevation of both bogs is taken from the 2020-2022 Wales Lidar DSM at 1-m resolution.

## 4. Results

### 4.1. InSAR-derived displacements from long and short temporal baseline networks

#### 4.1.1. Long temporal baseline networks

**Figure 6** shows the InSAR-derived surface displacement rates computed for Cor Fochno and Cors Caron from the long TBNs. The extended displacement rate maps for the areas around the bogs, including the reference points, can be found in Supplementary Materials (see **Figure S7-S8**). Observation points here are mainly obtained on man-made structures (i.e., buildings, etc.) and on the two bogs. In detail, the number of InSAR points on each peatland decreases outward from the centre, where there is near complete coverage, to the bog edges, where there are isolated “islands” of points (**Figure 6**).

On Cors Fochno, the long TBN results indicate that during the full observation period the centre of bog area had negative LOS displacements, at rates of up to  $\sim -6 \text{ mm}\cdot\text{yr}^{-1}$  (see **Figure 6a-b**). The bog edges, conversely, had positive LOS displacement rates of up to  $\sim +4 \text{ mm}\cdot\text{yr}^{-1}$ , with maximum values in the north-west. The LOS displacement pattern is not perfectly centred on the bog coverage: it is offset to north-east. Ascending and descending passes were broadly similar, even if incidence angles of the SAR geometries differ by a few degrees (ascending:  $34^\circ$ ; descending:  $39^\circ$ ) (see **Table 1**). Around the bog (i.e., in background areas), LOS displacement rates were not strictly equal and can vary with a factor of  $\sim 2$  (see **Figure S7** in Supplementary Materials).

**Table 1** Overview of InSAR-derived displacement rates in  $\text{mm}\cdot\text{yr}^{-1}$  computed on Cors Fochno (C.F.) and Cors Caron (C.C.), depending on the used networks (long-term and short-term) of interferograms. Standard deviations are given at  $1\sigma$ .

	Long TBN		Short TBN	
	<i>Ascending</i>	<i>Descending</i>	<i>Ascending</i>	<i>Descending</i>
<b>LOS velocity on C.F.</b>	-1.4±2.1	-0.3±2.1	-0.2±3.2	-0.3±2.1
<b>LOS velocity on C.F. background</b>	-2.2±4.3	-0.6±2.4	-13.2±10.7	-8.2±9.5
<b>LOS velocity on C.C.</b>	-2.1±1.4	-2.1±1.6	-9.2±3.1	-10.0±3.5
<b>LOS velocity on C.C background</b>	-1.8±4.0	-1.3±2.2	-12.0±10.8	-6.6±9.5

For Cors Caron, the long TBN results indicate that the bog had entirely negative LOS displacement rates, at a rate of  $\sim -8 \text{ mm}\cdot\text{yr}^{-1}$  in the bog centre (see **Figure 6c-d**). As for Cors Caron, the LOS displacement rate decreased toward the margins, but with few observations of positive LOS displacement rates (in the northeast of the western peat unit). For the north-western peat unit, the max. LOS displacement rate pattern was also not centred on the bog but shifted toward the north-western border. Results from the ascending and descending passes were again broadly similar (see **Table 1**). Around Cors Caron, LOS displacement rates are similar (see **Figure S8** in Supplementary Materials).

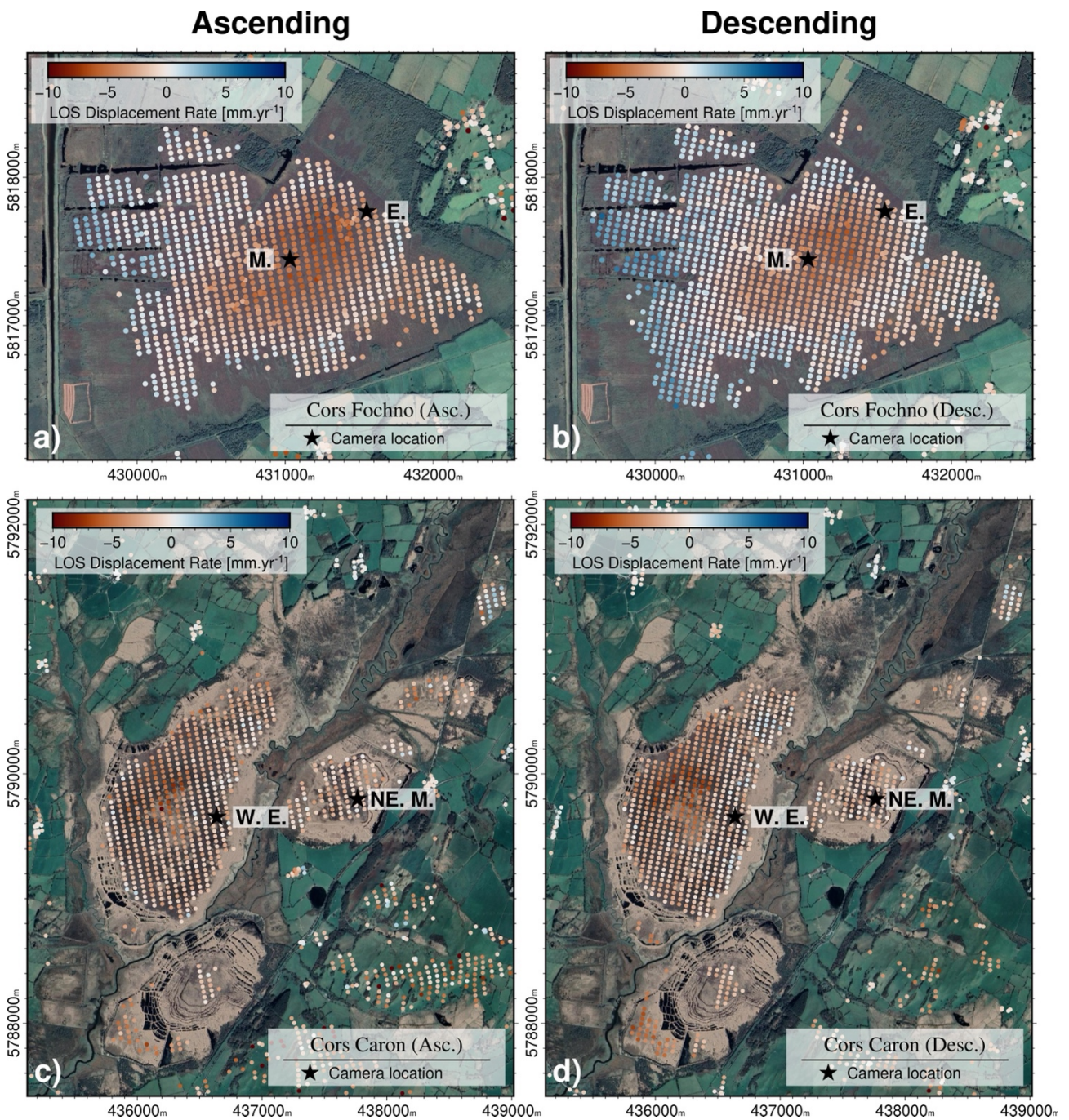


**Figure 6** InSAR-derived LOS displacement maps on the two Welsh peatlands from the long TBNs. **a)** Map of InSAR-derived LOS displacement rates at Cors Fochno for the ascending pass, and **b)** Map of LOS displacement rates at Cors Fochno for the descending pass. **c)** Map of InSAR-derived LOS displacement rates at Cors Caron, for the ascending pass. **d)** Maps of LOS displacement rates at Cors Caron for the descending pass. The maps are given in 30U UTM meters. Peat-camera locations are shown as black stars in each panel.

*The names of peat-camera stations are for Cors Fochno: M.: Middle, E.: Edge; and for Cors Caron: W. E.: West Edge and NE. M.: Northeast Middle. Optical images from Google Earth<sup>®</sup>.*

#### 4.1.2. Short temporal baseline networks

**Figure 7** shows the InSAR-derived displacement rates computed from the short TBNs. On Cors Fochno, the results from the short-term network were broadly the same as the results from long-term network, but with an increase in spatial noise (see **Figure 7a-b**). On Cors Caron, however, the results from the short-term network yielded greater LOS displacement rates (10's  $\text{mm}\cdot\text{yr}^{-1}$ ) compared to those from the long-term networks (3 - 5  $\text{mm}\cdot\text{yr}^{-1}$ ) (see **Table 1**). In addition, LOS displacement rates were very intense on the backgrounds of each peatland (see **Table 1** and **Figures S7-S8** in Supplementary Materials), such that each map of LOS displacement rates is affected by global offset of LOS displacement rates to negative rates. In addition, ascending and descending passes were abnormally different (see **Table 1**): especially for Cors Caron where no large horizontal displacements were expected.

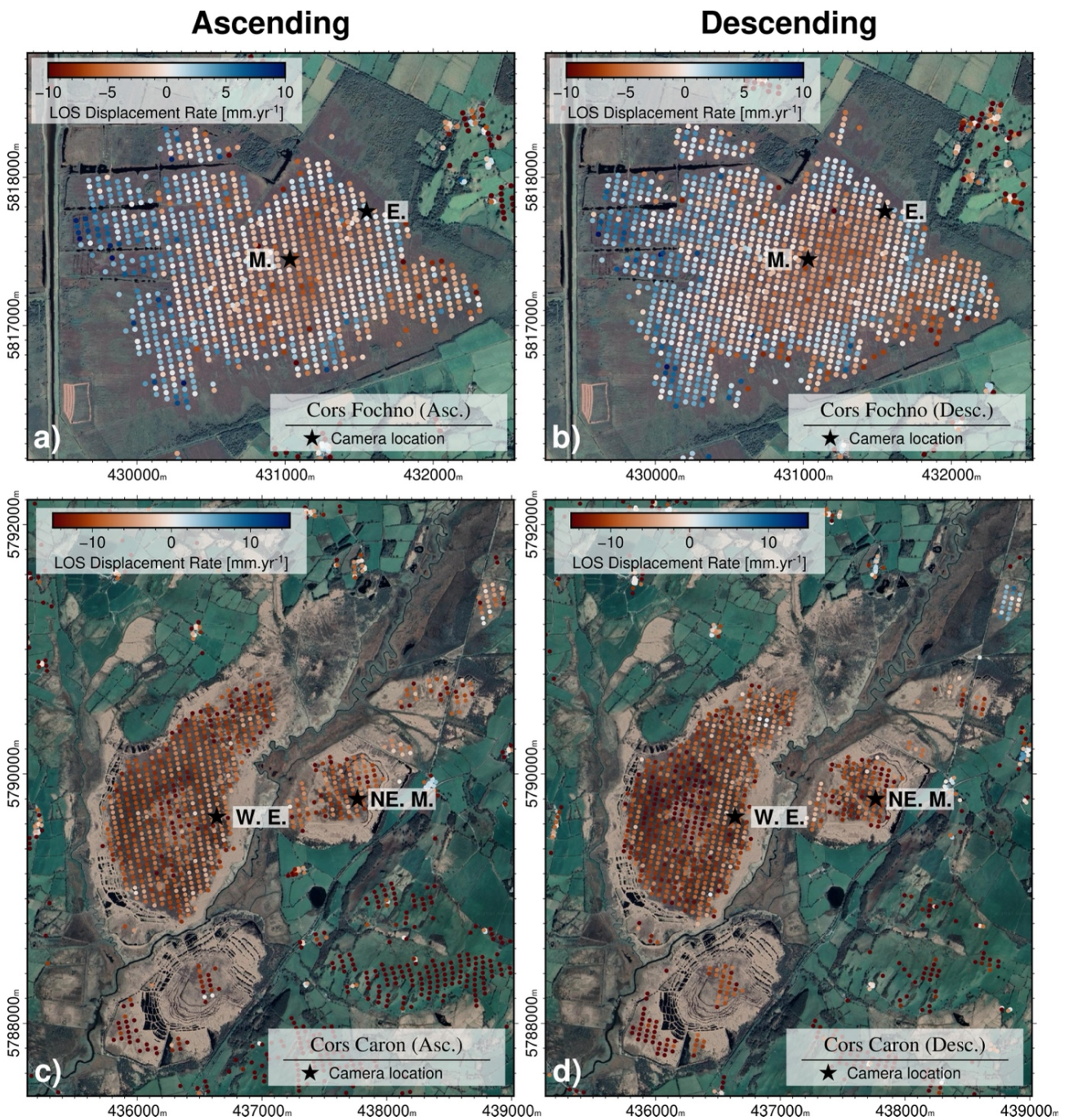


**Figure 7** InSAR-derived LOS displacement maps on the two Welsh peatlands from the short TBNs. **a)** Map of InSAR-derived LOS displacement rates at Cors Fochno for the ascending pass, and **b)** Map of LOS displacement rates at Cors Fochno for the descending pass. **c)** Map of InSAR-derived LOS displacement rates at Cors Caron, for the ascending pass. **d)** Maps of LOS displacement rates at Cors Caron for the descending pass. The maps are given in 30U UTM meters. Peat-camera locations are shown as black stars in each panel.

*The names of peat-camera stations are for Cors Fochno: M.: Middle, E.: Edge; and for Cors Caron: W. E.: West Edge and NE. M.: Northeast Middle. Optical images from Google Earth<sup>®</sup>.*

#### 4.1.3. Comparison of long and short TBNs with in-situ displacements

**Figure 8** shows the available time series of peat surface displacements as measured in-situ by the PeatCams and compared to the time series of InSAR-derived displacements at those same locations using either long-term or short-term networks. To enable comparison, the vertical displacements from the peat cameras were converted to those expected in the satellite LOS by a multiplication factor of  $\frac{1}{\cos(inc)}$ , where *inc* is the incidence angle ([Wright, 2004](#)). For Cors Fochno, both peat cameras show that the peat surface annually oscillates with an amplitude of around  $\pm 20$  mm, with the peat surface elevation higher in winter and lower in summer (see **Figure 8a-d**). The Middle peat camera also showed subsidence of  $-18 \pm 6.0$  ( $1\sigma$ )  $\text{mm}\cdot\text{yr}^{-1}$  over the whole period of observation (based on linear fit). The vertical velocity recorded by the Edge peat camera was  $+19.9 \pm 11.2$   $\text{mm}\cdot\text{yr}^{-1}$ . However, one must treat this estimate of long-term motion rate at this station with caution, because the measurement period is just over one year. On Cors Caron, the annual oscillations of vertical displacements had a lower amplitude (around  $\pm 10$  mm) (see **Figure 8e-h**). The velocities were  $3.1 \pm 0.4$   $\text{mm}\cdot\text{yr}^{-1}$  for the West Edge peat camera and  $-2.6 \pm 0.8$   $\text{mm}\cdot\text{yr}^{-1}$  for the Northeast Middle peat camera.

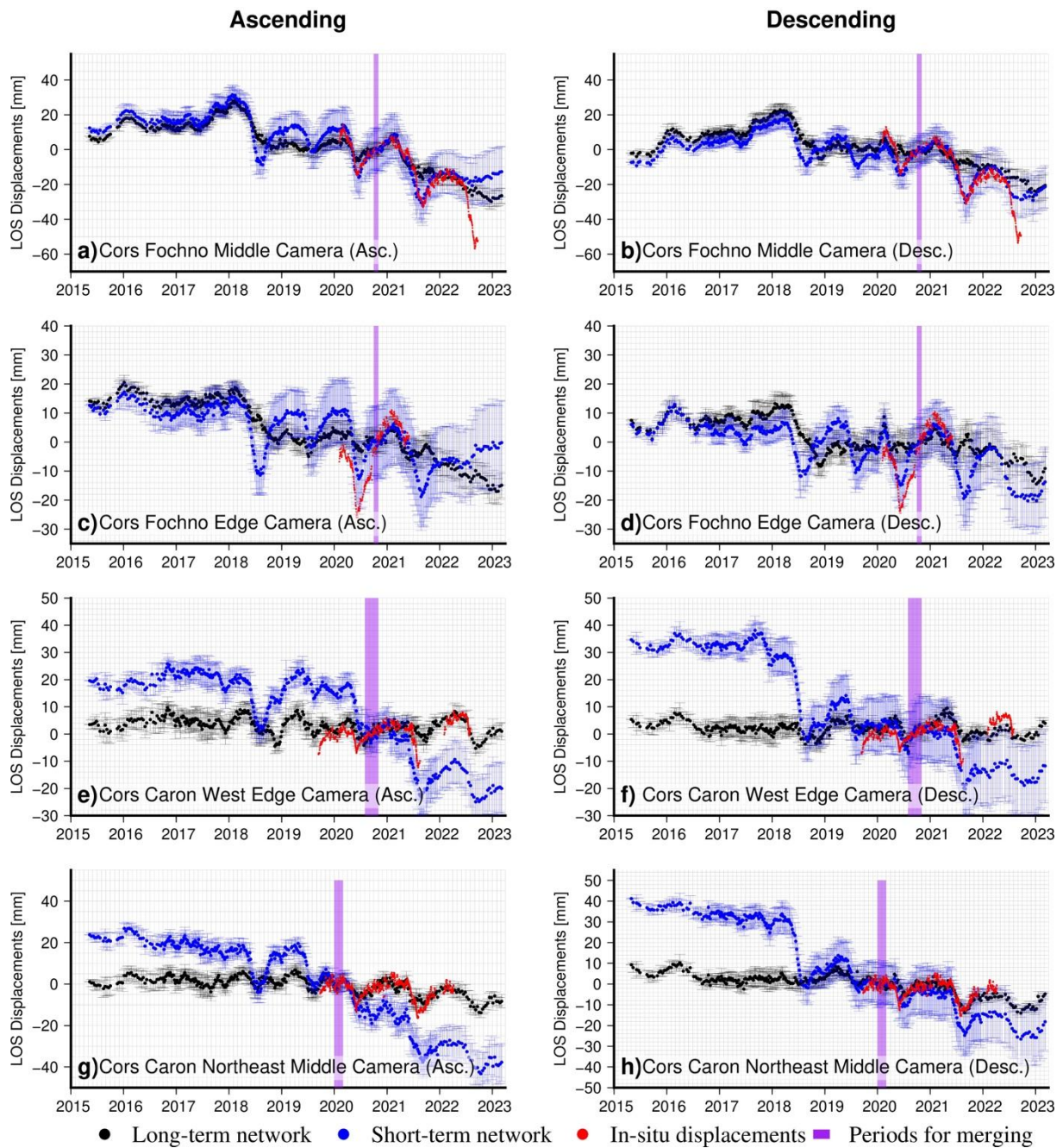


**Figure 8** Time series of InSAR and in-situ LOS displacements. **a)-g)** Times series of LOS displacements for all the used peat-camera stations with the time series computed from long-term and short-term networks. The InSAR-derived results are represented by black dots (long-term network) and by blue dots (short-term network). In-situ displacements are given in red. The purple polygons give the periods used to merge both relative time series. Asc.: ascending. Desc.: descending.

**Table 2** Overview of InSAR-derived LOS displacement times series computed on Cors Fochno (C.F.) and Cors Caron (C.C.), depending on the used networks of interferograms: i.e., the processing parameters are identical for all the calculations. The velocities at the peat camera locations are estimated on the durations of peat-camera time-series durations. Standard deviations are given at  $1\sigma$ .

		Short TBN		Long TBN	
		Ascending	Descending	Ascending	Descending
LOS displacement rates at the peat camera locations [mm·yr <sup>-1</sup> ]	C.F. Middle	-10.9±9.0	-8.5±8.0	-10.7±2.6	-6.8±0.9
	C.F. Edge	-0.5±10.8	9.0±7.7	-1.0±1.9	0.5±1.9
	C.C. West Edge	-14.9±2.9	-7.8±2.0	0.8±0.6	-0.4±0.8
	C.C. Northeast Middle	-16.8±2.5	-8.3±2.2	-2.8±1.2	-4.1±1.0
	Average Mismatch [mm·yr <sup>-1</sup> ]	7.5		3.2	
Pearson's coefficients at the peat camera locations	C.F. Middle	0.76	0.90	0.73	0.55
	C.F. Edge	0.89	0.87	0.72	0.61
	C.C. West Edge	0.79	0.78	0.54	0.41
	C.C. Northeast Middle	0.79	0.84	0.74	0.73
	Mean coefficient	0.83		0.63	

Regarding the InSAR-derived LOS displacement rates for the PeatCam locations, the results differ depending on the interferogram network used (**Figure 8**). For the two peatlands, the lowest mismatch (mean of deviations) of velocity for InSAR versus peat camera is obtained by using the long TBNs (see the upper part of **Table 2**). Consequently, on Cors Fochno and Cors Caron, the long TBNs appear to be the best interferometric networks to estimate the velocity of peat surface displacements.

On the other hand, the InSAR time series from long TBNs show systematic underestimation of LOS displacement oscillations as measured *in-situ*. Instead, the InSAR time series from short TBNs better match the annual oscillations of the in-situ displacements (see **Figure 8**). The Pearson's coefficient is used to define the correlation between the detrended InSAR-derived observations and the detrended *in-situ* measurements (see the lower part of **Table 2**). For the two peatlands, the highest coefficient is obtained by the short TBNs. Consequently, on Cors Fochno and Cors Caron, the short TBNs appear to be the best interferometric networks to estimate the sub-annual oscillation of peat surface displacements.

#### **4.2. InSAR results from combined long and short TBNs**

While the long-TBN results give accurate estimates of the multi-annual surface motion velocity, the short TBNs capture with the best accuracy the amplitude of sub-annual oscillations. Therefore, we consider a combined dataset from the 3D-unwrapping methods as the best compromise for both peatlands.

We create combined results for which: (1) the long-term LOS velocity is estimated by using the long TBNs; (2) the LOS displacements are estimated by using the short TBNs. Then, these combined datasets are used to compute the vertical and horizontal (East-West) components of displacements. The coverage of InSAR measurement points is low on the regional scale, respectively 50 and 17 points per km<sup>2</sup> for the processed areas for Cors Fochno and Cors Caron (see Supplementary Materials). On the two peatlands, however, the point density is far higher at around 160 points per km<sup>2</sup> (~180 for Cors Fochno and ~140 for Cors Caron).

#### 4.2.1. Vertical and horizontal components of multi-annual ground motion rate

On Cors Fochno, InSAR indicates that during the observation period the centre of bog area has undergone subsidence at rates of  $-7 \text{ mm}\cdot\text{yr}^{-1}$  (see **Figure 9a**). The bog edges have conversely undergone uplift of up to  $+5 \text{ mm}\cdot\text{yr}^{-1}$ , with maximum values in the north-west. The vertical displacement pattern is also not perfectly centred on the bog: it is offset to north-east. The results indicate an apparently consistent if small eastward horizontal long-term displacement on Cors Fochno (see **Figure 9b**). These apparent horizontal displacements may not be significant as their statistical distribution is  $0.85\pm 0.60 (1\sigma) \text{ mm}\cdot\text{yr}^{-1}$ . This is confirmed by the very high similarity of displacements from each pass during our computations from long-term networks, with similar incidence angles of the SAR geometries.

For Cors Caron, InSAR indicates that almost the entire bog has undergone subsidence, at up to a rate of  $-9 \text{ mm}\cdot\text{yr}^{-1}$  (see **Figure 9c**). The vertical displacement rate decreases toward the margins, but little or no uplift is observed. For the north-western unit, the vertical displacement rate pattern is also not centred on the bog but shifted toward the north-western border. Again, we do not observe significant horizontal displacement (**Figure 9d**) given the noisiness of the patterns in space and the measurement uncertainty ( $-0.13\pm 0.90 (1\sigma) \text{ mm}\cdot\text{yr}^{-1}$ ).

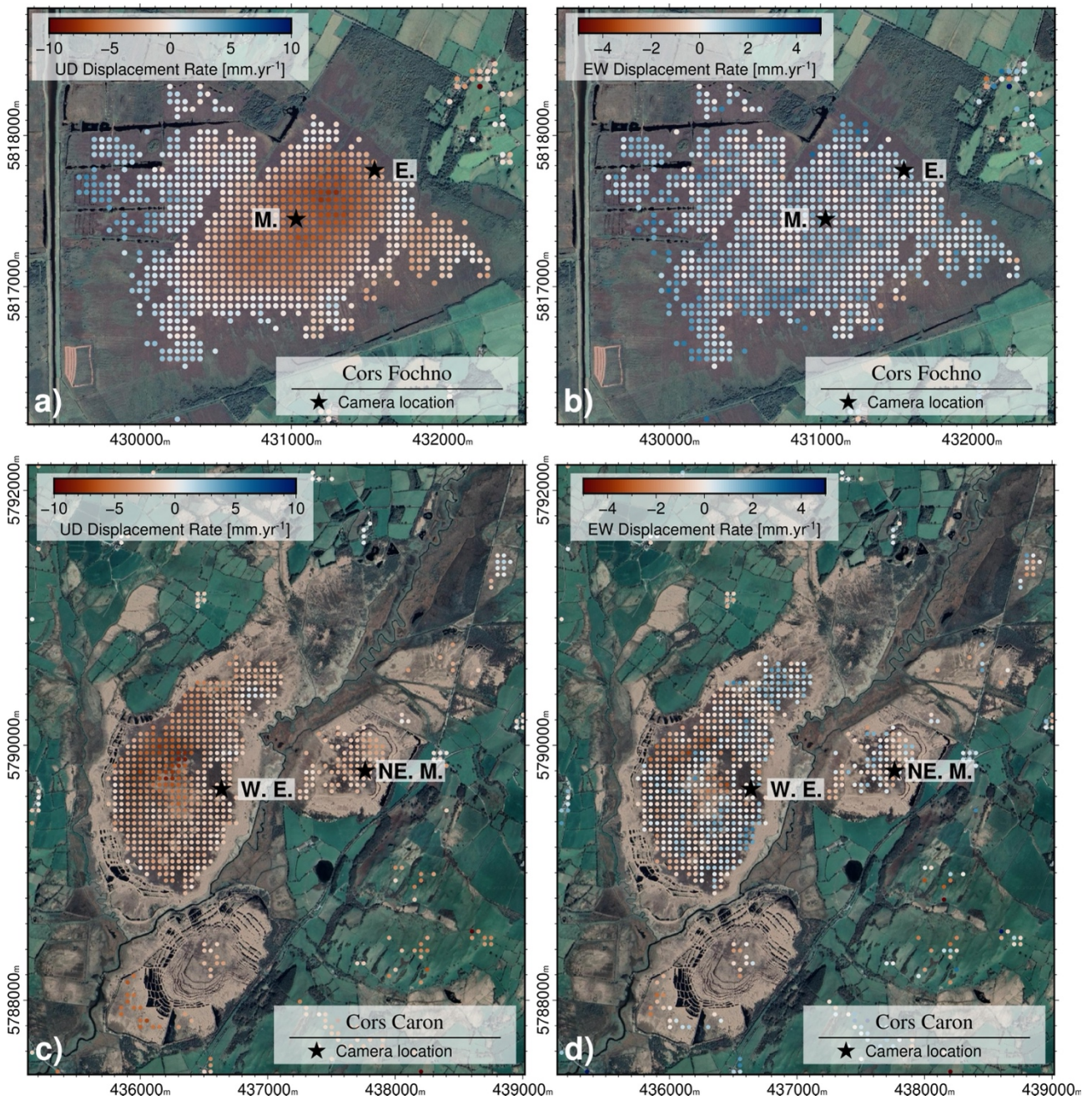


**Figure 9** InSAR-derived displacement maps on the two Welsh peatlands. **a)** Map of InSAR-derived vertical displacement rates at Cors Fochno, and **b)** Map of West-East displacement rates at Cors Fochno. **c)** Map of InSAR-derived vertical displacement rates at Cors Caron. **d)** West-East displacement rates at Cors Caron. The maps are given in 30U UTM meters. Negative UD implies subsidence; Negative EW implies westward motion. Peat-camera locations are shown as black stars in each panel. The names of peat-camera stations are for Cors

*Fochno: M.: Middle, E.: Edge; and for Cors Caron: W. E.: West Edge and NE. M.: Northeast Middle. Optical images from Google Earth®.*

#### 4.2.2. InSAR time series versus in-situ vertical displacements measurements

**Figure 10a-e** shows the time series of peat surface vertical displacements measured in situ by the cameras and those measured remotely by satellite InSAR. A brief description of horizontal displacements is given in Supplementary Materials Section 6. The peat camera data cover the period from late-2019 to late-2022, while the InSAR measurements – here reported for the area with a radius of 50 m of each peat camera location – span the years 2015-early 2023.

On the long term (i.e., ~8 years), the InSAR-derived time-series of displacements around the camera stations can be approximated by linear subsidence trends. These attain values, at  $1\sigma$  error, of:  $-5.0\pm 0.3$   $\text{mm}\cdot\text{yr}^{-1}$  (**Figure 10a**);  $-3.9\pm 0.2$   $\text{mm}\cdot\text{yr}^{-1}$  (**Figure 10b**);  $-3.1\pm 0.2$   $\text{mm}\cdot\text{yr}^{-1}$  (**Figure 10c**);  $-0.6\pm 0.2$   $\text{mm}\cdot\text{yr}^{-1}$  (**Figure 10d**); and  $-1.6\pm 0.2$   $\text{mm}\cdot\text{yr}^{-1}$  (**Figure 10e**). Such values are shown also on the maps in **Figure 9**. In detail, however, there is considerable non-linearity to the displacement evolution with time at both bogs. In the medium term (i.e., ~3 years), Cors Fochno and Cors Caron display subsidence or uplift trends either side of the summer of 2018. At Cors Fochno, the bog centre appears to have uplifted at  $\sim +5$   $\text{mm}\cdot\text{yr}^{-1}$  during 2015-2018, after which it appears to have subsided at around  $-8$   $\text{mm}\cdot\text{yr}^{-1}$  during 2019-2023. At Cors Caron, the medium-term displacement rates around the camera stations show apparent uplift between 2015 and 2018. On the short term (i.e., ~1 year), the InSAR data also show seasonal oscillations of typically  $\pm 5$ -20 mm, but with up to  $\pm 30$  mm reached at Cors Fochno in summer 2018.

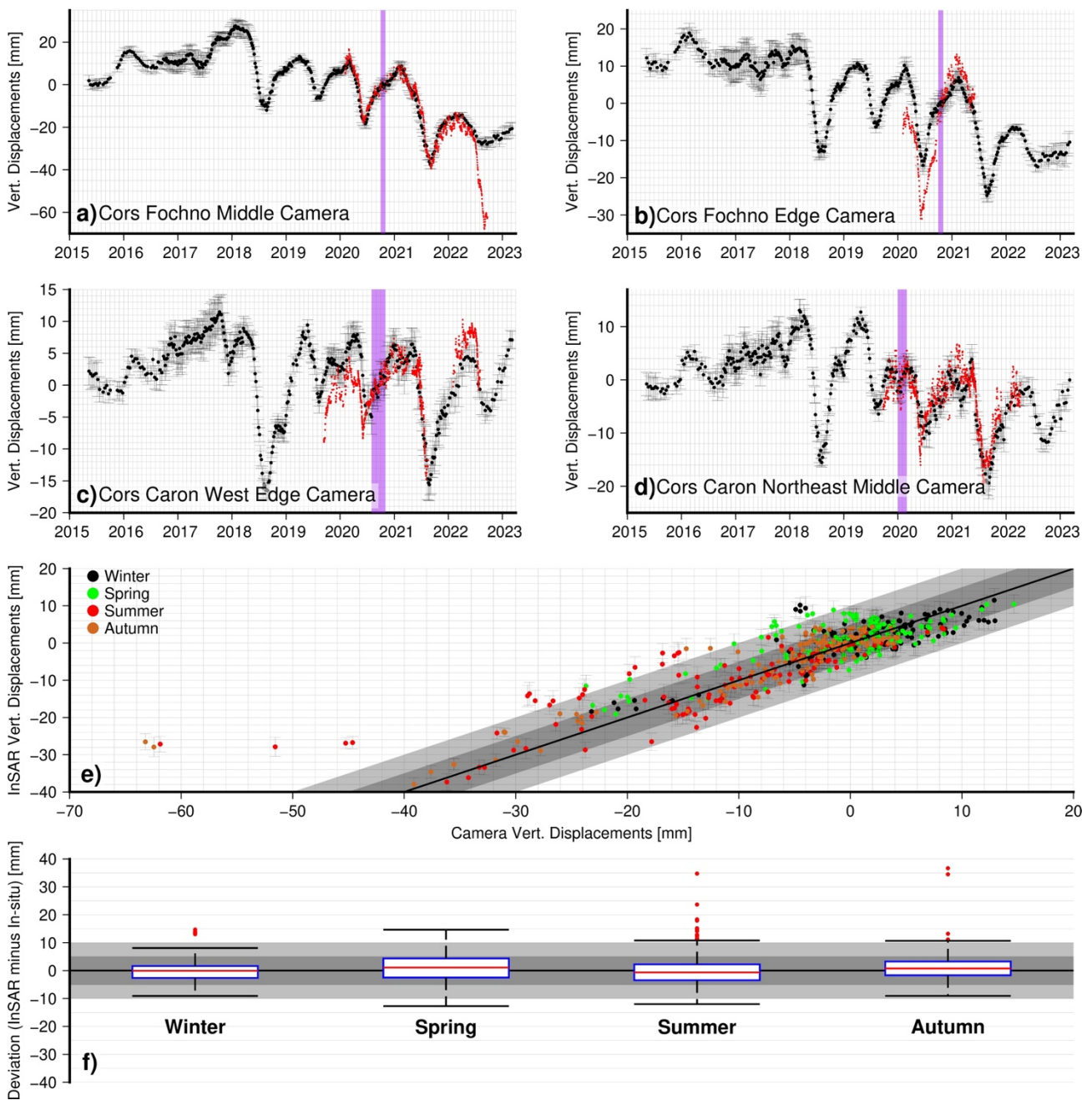


**Figure 10** Time series of InSAR and in-situ vertical displacements. **a)-d)** Times series of vertical displacements for all the used peat camera stations. The InSAR-derived results are represented by black dots and in-situ with red dots. The purple polygons give the periods used to merge both relative time series. **e)** Correlation plot between InSAR-derived and in-situ displacements, classified by season. **f)** Boxplots of deviations (InSAR displacements minus in-situ displacements), classified by season. The grey polygons in **e)** and **f)** give the bounds at 5 mm and 10 mm.

The *in-situ* peat camera data show good agreement with the InSAR data (**Figure 10a-d**). This is both in terms of the medium-term surface motion rate and in terms of the phase, period and amplitude of the annual (seasonal) oscillations. The average mismatch of the InSAR and *in-situ* velocities for all the stations is  $5.6 \text{ mm}\cdot\text{yr}^{-1}$  (**Table 3**). The amplitude of surface oscillation as measured by InSAR is well matched to the *in-situ* data for the middle cameras on each bog. The surface oscillation amplitude is underestimated by InSAR for the edge cameras on each bog, especially for the Cors Fochno Edge PeatCam station (maximum mismatch of 15 mm in the 2020 summer season). Given that the medium-term rate of motion can be strongly affected by shorter-term variation and the length of the observation period, it is noteworthy that the average mismatch for the *in-situ* and InSAR motion rates decreases to  $0.8 \text{ mm}\cdot\text{yr}^{-1}$  if the shorter-term Cors Fochno Edge peat camera station is excluded. This value is similar to conventional uncertainty ranges associated with InSAR velocity (i.e.,  $\pm 1 \text{ mm}\cdot\text{yr}^{-1}$ ) ([Hanssen, 2001](#); [Osmanoğlu et al., 2016](#)).

**Table 3** Velocity of vertical displacements during the peat camera observation periods and Pearson's coefficients between the InSAR displacement and the *in-situ* displacements, for Cors Fochno (C.F.) and Cors Caron (C.C.).

	Peat camera velocity of vertical displacements [mm·yr <sup>-1</sup> ]	InSAR-derived velocity of vertical displacements [mm·yr <sup>-1</sup> ]	Pearson's coefficient
<i>C.F. Middle</i>	$-18.0 \pm 6.0(1\sigma)$	$-12.3 \pm 11.8(1\sigma)$	0.85 ( $p\_value < 0.001$ )
<i>C.F. Edge</i>	$19.9 \pm 11.2(1\sigma)$	$0.1 \pm 0.02(1\sigma)$	0.92 ( $p\_value < 0.001$ )
<i>C.C. West Edge</i>	$3.1 \pm 0.4(1\sigma)$	$-2.9 \pm 2.6(1\sigma)$	0.88 ( $p\_value < 0.001$ )
<i>C.C. Northeast Middle</i>	$-2.6 \pm 0.8(1\sigma)$	$-4.7 \pm 2.9(1\sigma)$	0.84 ( $p\_value < 0.001$ )

---

**Average Mismatch**  
**[mm·yr<sup>-1</sup>]**

**5.6**

Statistically, there is no argument to reject the hypothesis of similarity between InSAR-derived and *in-situ* displacements. On **Figure 10e**, the correlation plot shows the relationship between *in-situ* and InSAR-derived displacements, classified by season. The Pearson's coefficients are  $> 0.80$  for all stations, with an average coefficient at 0.87 (see **Table 3**). Some 76 % of the point deviations are  $< 5$  mm, whereas 93 % are  $< 10$  mm. The distribution of deviations is normal and has the following parameters:  $\mu=1.0$  mm;  $med=0.1$  mm;  $\sigma=5.4$  mm, which are characteristics of distribution for InSAR uncertainty. Conversely, the distributions are not normal in summer and spring, with most outliers occurring in these periods. In **Figure 10f**, the boxplots show that all deviations are lower than the conventional uncertainties. In Supplementary Materials, the results from the 2D-unwrapping method are briefly described (and see Discussion Section).

### **4.3. InSAR surface displacement versus groundwater level change**

From **Figure 2** and for Cors Fochno and Cors Caron, we identify several main oscillations of groundwater levels. These are associated with high evapotranspiration rates during summer periods. Overall, the post-2020 summers were particularly dry and associated with large variations in groundwater levels whereas the 2015-2017 period includes the 4<sup>th</sup>, 3<sup>rd</sup> and 2<sup>nd</sup> wettest April-August periods chronologically for the period 2010-2023. In details, summer 2018 was a drought period with around a -40% of rainfall anomaly and +1.5-2°C temperature, summer 2019 had no significant rainfall anomaly but a +1.5°C temperature anomaly, and summer 2020 has a -20% rainfall anomaly and +1.5-2°C temperature anomaly (all relative to long-term means). In winter, a large negative rainfall anomaly in fall/winter 2016-2017 ( $< -50\%$ ), without an accompanying temperature anomaly, did not lead to water level drawdown.

**Figure 11** shows selected times series of InSAR-derived vertical displacements and groundwater data for Cors Fochno. Again, the InSAR data represent an average time series of all InSAR points within a 50-m radius of each measurement site (see **Figure 1** for locations). Unfortunately, groundwater data for Cors Caron are missing for most of the InSAR observation period. The full datasets for both bogs are given in **Figures S13, S14 and S15** in Supplementary Materials. The stations selected for Cors Fochno in **Figure 11** are broadly representative of differing medium- to long-term trends of peat surface displacement there, and these stations have complete records for the entire duration of the InSAR observation.

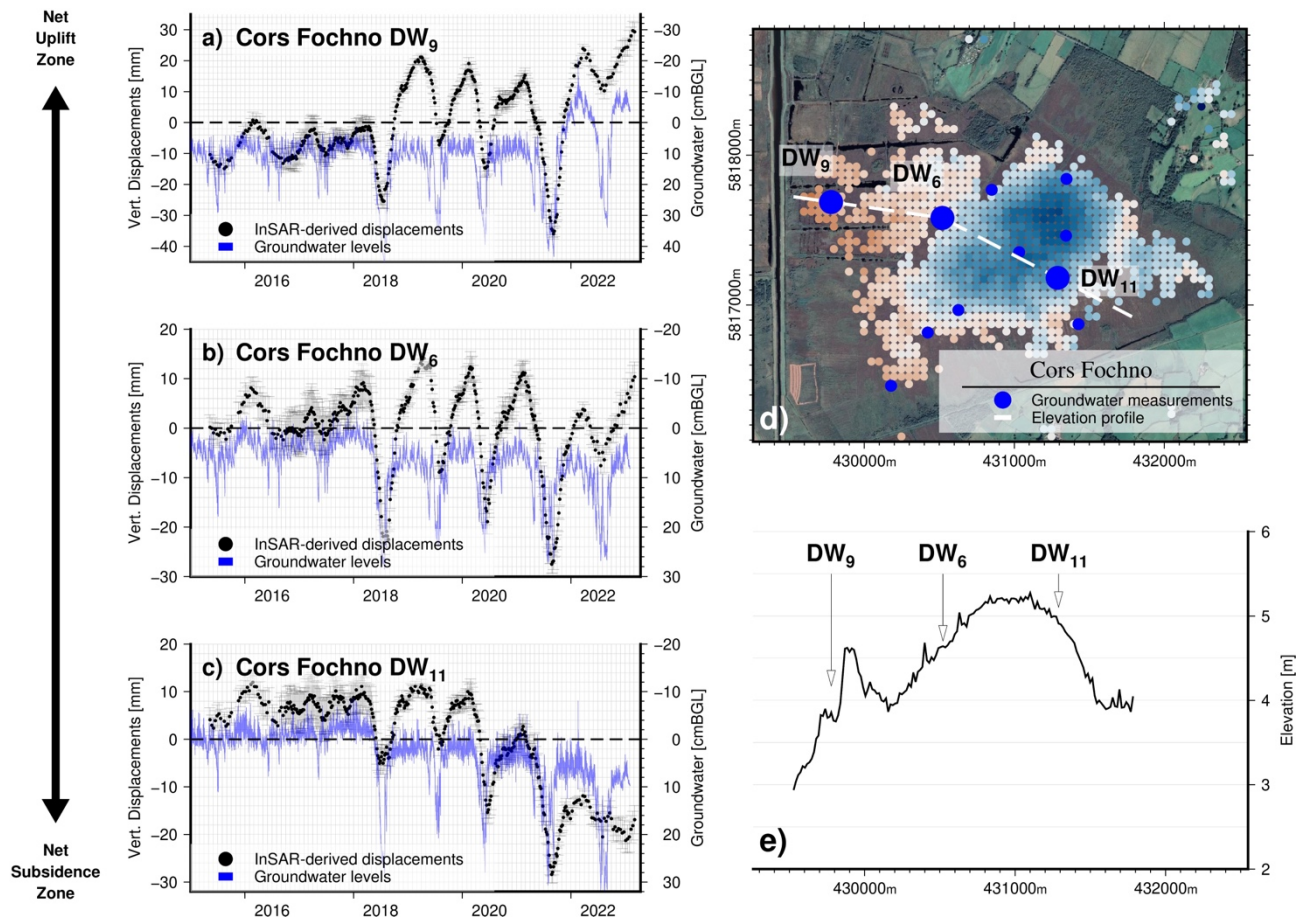


**Figure 11** Selected time series of InSAR-derived vertical displacements and groundwater levels. **a-c)** Time series of InSAR-derived vertical displacements and groundwater levels for the three selected groundwater stations on Cors Fochno. Note that the values on the vertical axes of each plot differ by a factor of 10 – i.e.

*InSAR-derived peat surface displacements are approximately ten times less than the groundwater level changes. d) Map of InSAR-derived vertical displacement rates at Cors Fochno with the locations of groundwater-level stations. Optical images from Google Earth<sup>®</sup>. e) Lidar elevation profile along the selected groundwater stations.*

There is a close relationship between the short-term (annual) variation in the InSAR-derived surface displacement and the seasonal rise and fall of the groundwater table at Cors Fochno (**Figure 11**). In general, the groundwater level changes precede the corresponding motions of the peat surface. Moreover, the recovery of the groundwater level to a peak value occurs sooner than the corresponding recovery of the surface level. Thus, the groundwater and bog surface oscillations are slightly out of phase, with the peat surface lagging the water table by several days/weeks.

Within the area of Cors Fochno marked by long-term subsidence, the average groundwater levels are more elevated in the period 2015-2018, and drop by 5-15 cm on average in the period 2018-2021 (see **Figure 11a-b**). This results from the winter peaks of groundwater levels being higher, and from the summer troughs in groundwater levels being less far pronounced in the period 2015-2018 than in the subsequent period 2018-2021. Within the area marked by long-term uplift, on the other hand, there is a smaller drop in the average groundwater level after 2018. The summer troughs in groundwater level are again more marked after 2018, but the winter peaks are a similar level over the entire 2015-2021 period.

**Figure 12a** gives correlation plots between InSAR-derived vertical displacement rates and groundwater level change rates (corrected from peat surface displacements) both Cors Fochno and Cors Caron. The rates are calculated at each measurement station by simple linear fit to each time series. For Cors Caron, only selected stations, for which the lack of groundwater measurements does not affect our computation of rates (stations CC<sub>2</sub>, CC<sub>3</sub>, CC<sub>4</sub>, CC<sub>14</sub>, CC<sub>15</sub>, CC<sub>18</sub>, CC<sub>19</sub>), are presented

here. There is not a clear relationship between the long-term linear change in groundwater level and the long-term linear displacement rate of peat surface motion.

**Figure 12b** (and **Figure S13** in Supplementary Materials) shows the relationship between the InSAR-derived peat surface displacement and the groundwater levels for Cors Fochno. **Figure 12c** shows the similar relationship for Cors Caron from the selected stations. For Cors Fochno, the factor between groundwater level change and peat surface displacement is  $1.00 \pm 0.02$  ( $1\sigma$ ) ( $R_{ad}^2 = 0.45$ ). For Cors Caron the factor is  $0.63 \pm 0.02$  ( $1\sigma$ ) ( $R_{ad}^2 = 0.36$ ). The amplitudes of InSAR estimated bog surface oscillation therefore relate to those of the groundwater level oscillation with a ratio of roughly 10:1 or 20:1 – i.e., a 20 mm change in groundwater level produces a roughly 1-2 mm change in peat surface level.

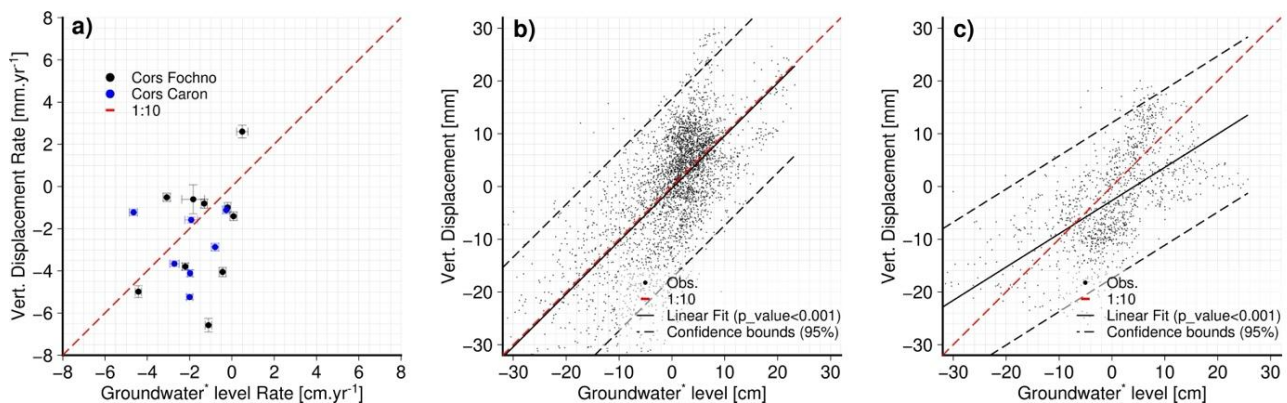


**Figure 12** Comparison between InSAR-derived displacements, groundwater levels and temporal rates on Cors Fochno and Cors Caron. **a)** Relationship between groundwater level long-term rates and long-term vertical displacement rates. **b-c)** Relationship between peat surface displacements and groundwater levels on Cors Fochno and Cors Caron. \* Corrected from peat surface displacements. In c) there is a slight offset of -3 mm between the regression line and the origin, as the time series are not centred exactly at the same period.

#### 4.4. InSAR displacements versus bog geometry

Displacement rates at the two bogs generally increase with peat elevation (from Lidar survey): proxy of the peat dome. (**Figure 13**), such that the highest displacement rates are located on the summit of peat domes. For Cors Fochno (**Figure 13a**), at first order, there is a negative 2-order power relationship between these two parameters with  $R_{ad}^2 = 0.74$ . For Cors Caron (**Figure 13b**), a weaker correlation is observed with  $R_{ad}^2 = 0.28$ .

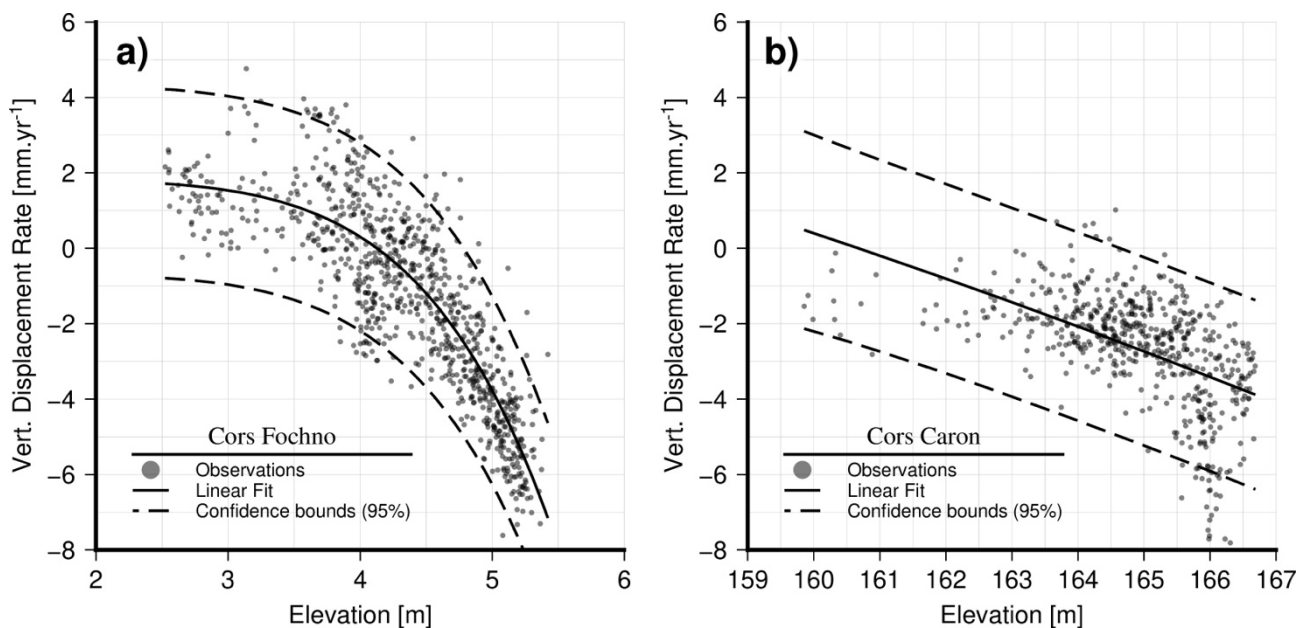


**Figure 13** Relationships between InSAR-derived displacements and Lidar elevations. **a)** Relationship between peat surface elevation and vertical displacement rates for Cors Fochno. **b)** Relationship between peat surface elevation and vertical displacement rates for Cors Caron.

On **Figure 14** and for Cors Fochno, slight differences can be observed between the peat surface elevations by Lidar (2020-2022) and the in-situ measurements (2009). The Lidar peat surface elevations mainly are lower than the elevations measured by in-situ measurements.

In addition, displacement magnitudes and rates at the two bogs generally increase with in-situ peat thickness (**Figure 14**), such that the highest displacement rates are located where peat thickness is

greatest. This is clearest for the north-south profile through Cors Fochno (see **Figure 14c**), less so in the W-E profile (see **Figure 14f**). A broadly similar relationship can be seen over Cors Caron (see **Figure 14e**). For Cors Fochno (**Figure 15a**), at first order, there is a negative linear relationship between these two parameters, consistent with the profiles, with a slope of  $-2.6 \pm 0.4$  ( $1\sigma$ )  $\text{mm} \cdot \text{yr}^{-1} \cdot \text{m}^{-1}$ ;  $R_{ad}^2 = 0.42$ ; and slope  $p$ -value  $< 0.001$ . For Cors Caron (**Figure 15b**), a weaker correlation is observed with a slope of around  $-0.6 \pm 0.3$  ( $1\sigma$ )  $\text{mm} \cdot \text{yr}^{-1} \cdot \text{m}^{-1}$ ;  $R_{ad}^2 = 0.26$ ; slope  $p$ -value = 0.020.

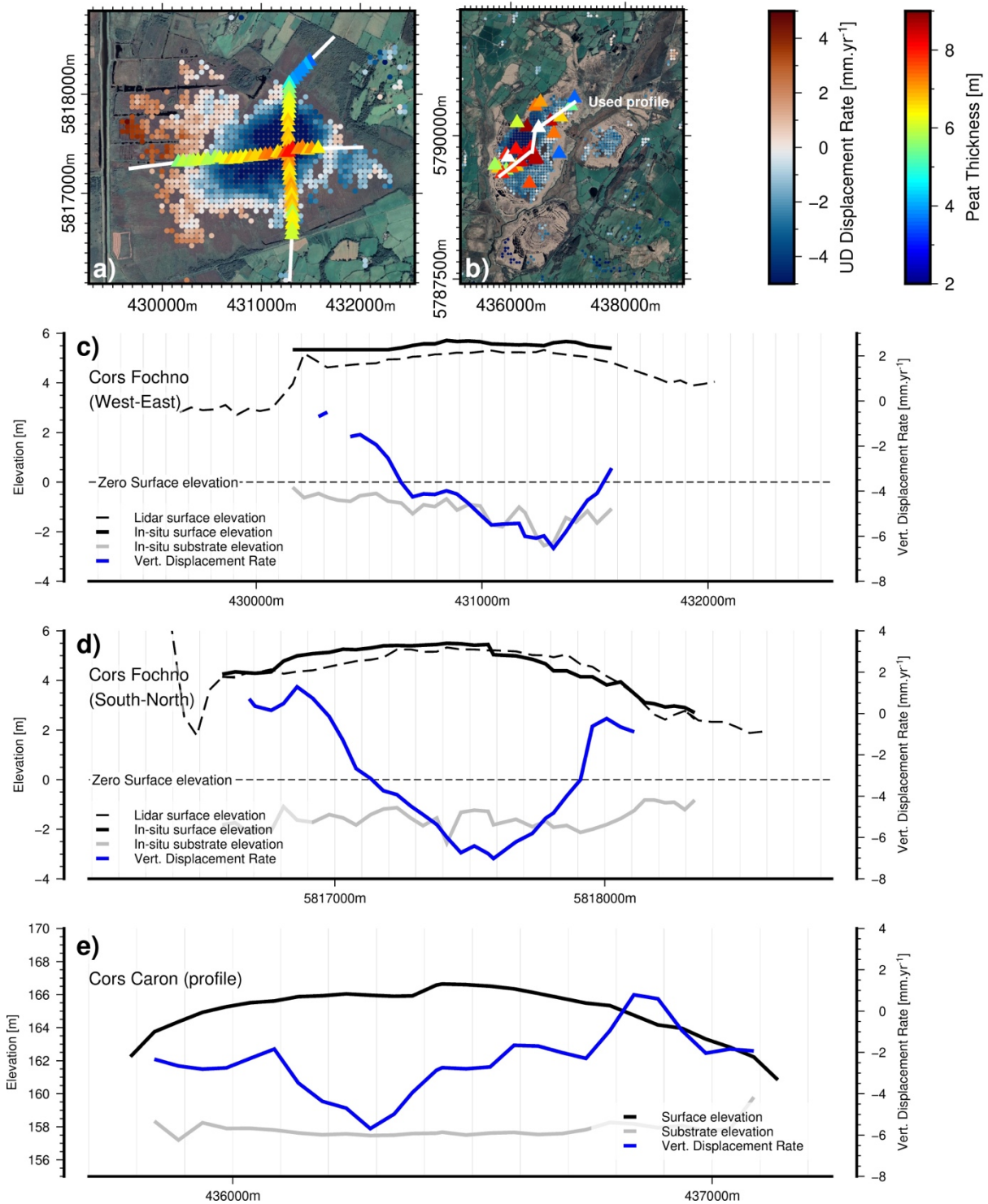


**Figure 14** Peat thickness and elevation data. **a)** Map of vertical displacement rates with thickness measurements for Cors Fochno represented by triangles. **b)** Map of vertical displacement rates with thickness measurements for Cors Caron represented by triangles. **c)** West-East cross section on Cors Fochno with

vertical displacement rates. **d)** South-North cross section on Cors Fochno. **e)** Similar for Cors Caron profile. The maps are given in 30U UTM meters. Optical images from Google Earth®.

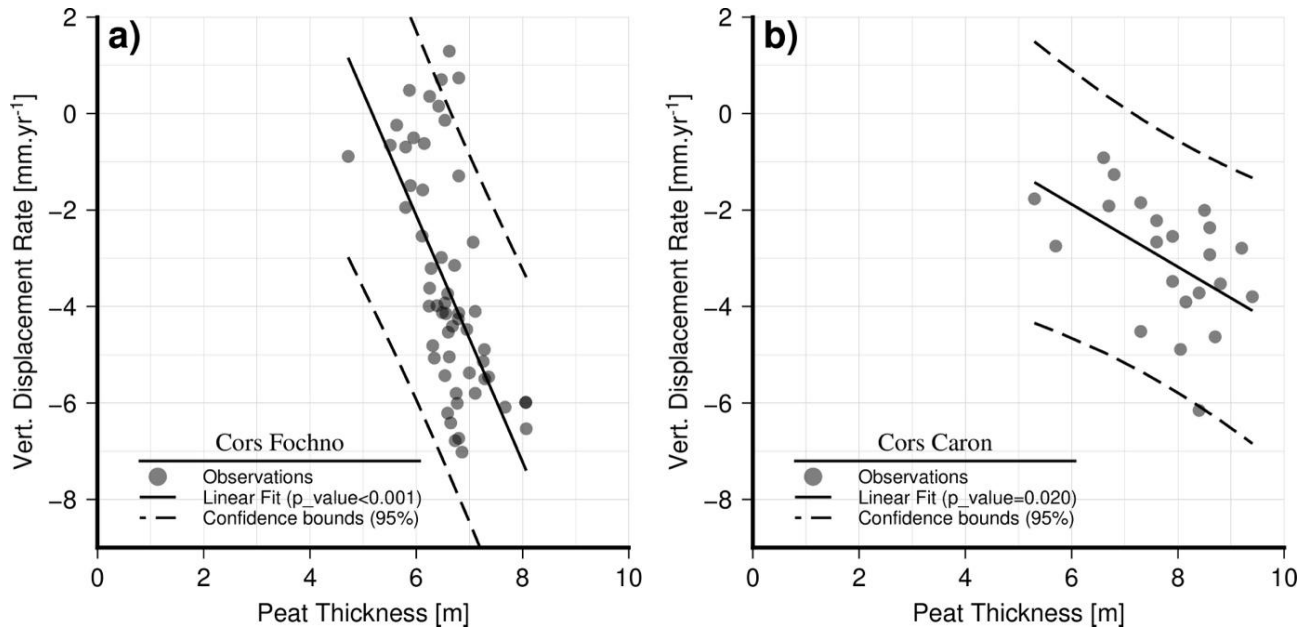


**Figure 15** Relationships between InSAR-derived displacements and peat thickness. **a)** Relationship between peat thickness and vertical displacement rates for Cors Fochno. **b)** Relationship between peat thickness and vertical displacement rates for Cors Caron.

## 5. Discussion

### 5.1. Ground validation of InSAR displacements from in-situ displacements

The new methodology proposed here of computing InSAR displacements by combining results from long and short TBNs is designed to preserve the long-term (multi-annual) trend of peatlands surface motion while also mitigating the underestimation of short-term (annual) displacement oscillations. From *in-situ* measurements of displacements at equivalent temporal resolution and precision, we have demonstrated the overall success of this method for relatively intact raised peatlands. Moreover, our

study offers a detailed ground validation of InSAR-derived peat surface displacements to date, based on the newly developed camera-based instruments for *in-situ* measurements.

[Marshall et al. \(2022\)](#) recently undertook a detailed ground validation of InSAR data at two blanket peatland sites in Scotland by using precise levelling of combinations of fixed or floating benchmarks: a 1 km<sup>2</sup> lowland site (6 fixed, 48 floating) and 1 km<sup>2</sup> upland site (7 fixed, 49 floating). The benchmarks were deployed in 7 clusters per site. The benchmarks were surveyed 16 and 10 times, respectively, over an 18-month observation period in 2017-2019. For both [Marshall et al. \(2022\)](#) and our study, comparison of multi-annual rates is not straightforward given the short duration of *in-situ* time-series and the amplitude of annual oscillations. The average mismatch of their InSAR motion rate to the *in-situ* motion rate was  $-9.9 \text{ mm}\cdot\text{yr}^{-1}$  for all 14 clusters; ours was  $5.6 \text{ mm}\cdot\text{yr}^{-1}$  for 4 sites. In detail the absolute mismatch of the results reported by [Marshall et al. \(2022\)](#) ranged from  $0 \text{ mm}\cdot\text{yr}^{-1}$  to  $42 \text{ mm}\cdot\text{yr}^{-1}$ ; ours ranged from 2 to  $20 \text{ mm}\cdot\text{yr}^{-1}$ . [Marshall et al. \(2022\)](#) noted that most of their ground motion rates from InSAR, although of the same sign as the *in-situ* rates, consistently underestimated the corresponding rates measured *in-situ*. We do not see a consistent underestimation by InSAR of the *in-situ* surface displacement rate, although we have a similar range of mismatch, and we have a smaller number of *in-situ* stations. Rates from InSAR and *in-situ* measurements are within uncertainty for two out of four stations (Cors Fochno Middle and Cors Caron East Middle) (**Table 3**); the others represent *in-situ* time-series that are either shorter (Cors Fochno Edge) or less complete (Cors Caron West Edge).

InSAR validation efforts for other geological settings – e.g., volcanoes, urban environments ([Ferretti et al., 2007](#)) – typically involve *in-situ* time-series that are much longer and involve ground motions that are of greater magnitude and more linear (or less oscillatory) than those recorded to date for peatlands. Thus, the mismatch between *in-situ* and long-term InSAR displacement rates at peatlands

will likely be reduced when longer time-series of *in-situ* displacement data (and more ground stations) are acquired.

On the other hand, we see a much closer agreement between the amplitude of peatland surface oscillation (“bog breathing”) measured *in-situ* and by InSAR. *In-situ* measurements of surface motion obtained by [Marshall et al. \(2022\)](#) show a range of annual elevation change of 10-60 mm (with one outlier of 120 mm), which is similar to the 10-40 mm range measured at our study sites. They observed a maximum decrease of the peat surface elevation in summer of 2018, which is also similar to our observations for the summers of 2018-2022. The Pearson’s coefficients from the results of [Marshall et al. \(2022\)](#) range from ~ 0.2 (upland site) to ~ 0.5 (lowland site); ours range from 0.8 to 0.9 on Cors Fochno and Cors Caron. The low and intermediate values of Pearson’s coefficient in the Marshall et al. 2022 study are mainly related to underestimation of InSAR-derived displacements during the drought period of 2018. The greater Pearson’s coefficient values reflect the fact we achieved closer match with the seasonal oscillation of displacement, even in the summer periods, which we attribute to our use of the combined network approach (see **Figure 16**).

In addition, [Tampuu et al. \(2022\)](#), which also undertook a ground validation of InSAR data on boreal peatlands on shorter period (July to October 2016). They show the same difficulties to obtain actual peat surface displacements on a raised bog in Estonia with similar *in-situ* technique than [Marshall et al. \(2022\)](#). With a very short period of observation (4 months), they propose to use only 6-day interferograms to observe relative peat surface change. However, with 1-2 years of *in-situ* measurements, we show that the use of short-TBN should not allow to capture the long-term and medium-term displacement rates of peat surface.

In summary, we achieve a robust ground validation of seasonal displacement oscillation estimated on temporal peatlands with InSAR. The validation of long-term is less robust because of peat surface

This manuscript is a non-peer reviewed preprint and has been submitted for publication in Remote Sensing of Environment. Please note that subsequent versions of this manuscript may have different content. Please feel free to contact any of the authors; we welcome feedback.

oscillations and the limited time series of data currently available. The estimation of rate by standard linear regression is strongly affected by the seasonal oscillation and is thus highly sensitive to the length of time series. Long-term rates of surface motion at peatlands derived by InSAR or *in-situ* methods from time-series of less than ~3 years duration should therefore be treated with caution; an analysis of long-term subsidence data from Indonesia excluded all records of less than four years duration for this reason ([Evans et al., 2019](#)). On the other hand, the *in-situ* data show that the seasonal oscillations of peatland surface displacement are well recovered by InSAR, and thus validation of long-term rates from InSAR should be feasible with longer-term time-series of *in-situ* measurements.

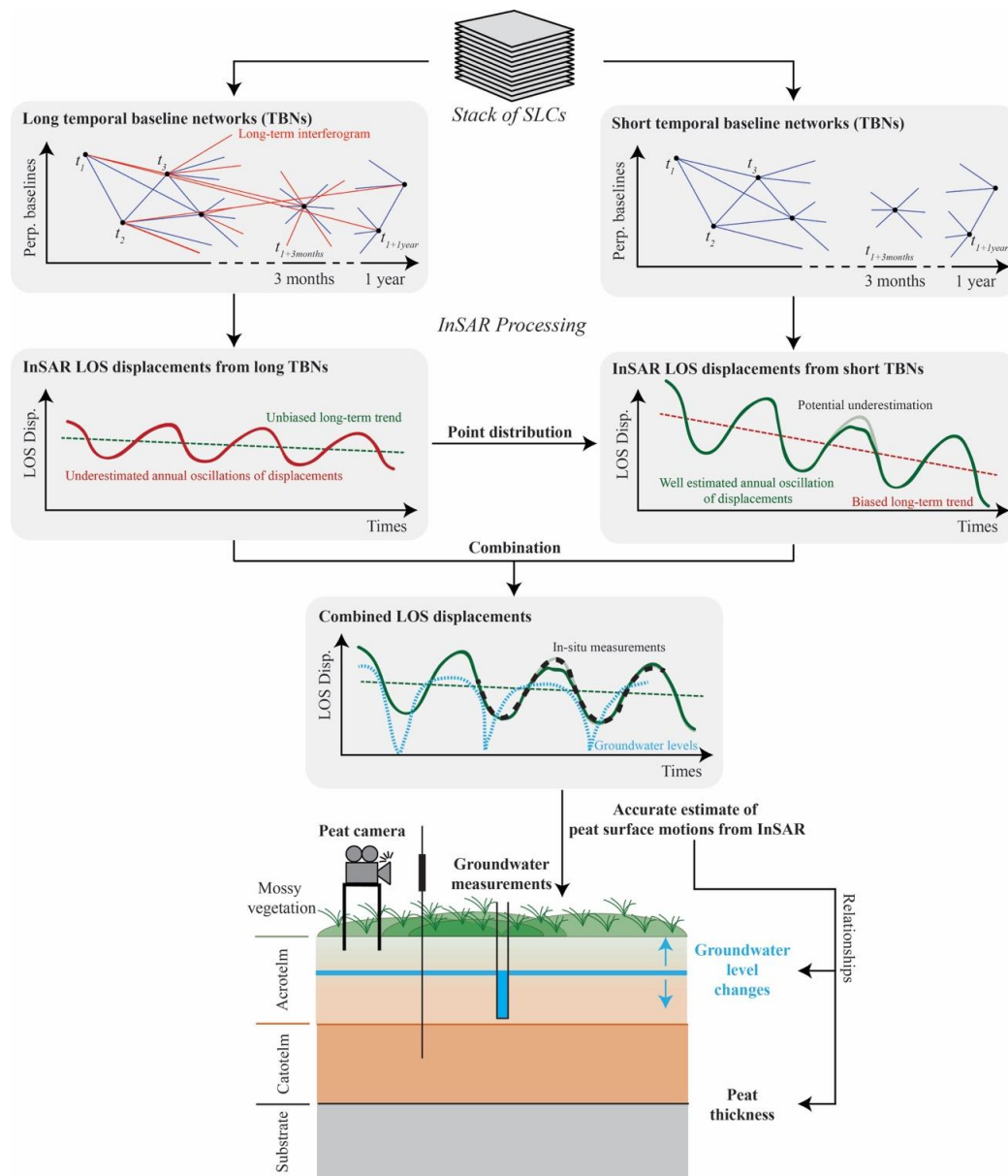


**Figure 16** Illustration of the “combined” InSAR methods to capture InSAR-derived peat surface displacements on temperate raised bogs (in upper part). In lower part, illustration of relationships extracted from InSAR-derived peat surface displacements and in-situ measurements.

## 5.2. Selection of long temporal-baseline network and unwrapping method

The proposed long TBN by [Ansari et al. \(2021\)](#) is not the unique solution to mitigate the bias of InSAR displacement velocity: another possibility is to use a Delaunay network ([De Luca et al., 2022](#)).

Delaunay networks have been tested during the computations, but this network type did not have the best results regarding the velocities and annual oscillations of LOS displacements ( $R=0.77$ ). These results therefore have intermediate precision and accuracy between long and short TBNs (see **Figures S7-S9** in Supplementary Materials).

The IPTA method uses a 3D-unwrapping method to unwrap the interferograms. This method can have limitations when displacement rates (or displacements) are high on a single interferogram ([Werner et al., 2003](#)). However this limitation mainly occurs with the short TBNs. Our comparisons between 3D-unwrapping and 2D-unwrapping methods, with the short TBNs, show that the results are very similar and that the 3D-unwrapping method seems slightly precise compared to the 2D-unwrapping method. Pearson's coefficients between displacements from 2D- and 3D-unwrapping methods vary from 0.79 to 0.86 – maps and time series of these results are given in Supplementary Materials (see **Figures S7-S10**). Finally, our results show that similar ground validation of InSAR-derived displacements can be done if the combined datasets are created from the short TBNs using the 2D unwrapping (see **Figures S12** in Supplementary Materials).

### **5.3. Sources of phase bias on displacement rates using the short TBNs**

The understanding of phase-bias sources is a current challenge (e.g., [Ansari et al., 2021](#); [De Zan et al., 2015](#); [Molan et al., 2020](#); [Zheng et al., 2022](#)). In this study, the velocity bias on displacement rates does not show the same variation on peat soils for Cors the two peatlands. The expected decrease in velocity deviations with the use of long TBNs is mainly observed on Cors Caron. However, the average coherences of InSAR stacks are not similar. The InSAR coherence is around 0.5-0.6 on Cors Fochno while this value decreases up to 0.3-0.4 for Cors Caron (the coherence of short TBNs always is, by definition, better than the coherence of long-term networks). This observed relationship could link the deviations in velocity bias to the InSAR coherence on peatlands.

In addition, our analysis of InSAR-derived datasets assumes that the phase biases mostly affect displacement rates and have no effects on short-term displacements. Further investigations of relationships between biases and time series should be done to verify this assumption on peat soils such as an estimation of phase biases for each peatland (e.g., [De Zan et al., 2015](#); [Molan et al., 2020](#); [Zheng et al., 2022](#)).

#### **5.4. Possible causes of remaining deviations in annual oscillations**

Unexplained small drought-season deviations could be accounted for by changes in soil moisture ([Zwieback et al., 2017](#)). Soil moisture changes of peat soils can be high during the summer, but are relatively low during the winter and intermediate seasons. Some previous studies have directly investigated the relationships between InSAR phase and soil moisture (as opposed to water table depth), using L-band data. The amplitude of Sentinel-1 SAR images is also currently used to map soil moisture at low resolution (1-km spatial resolution) (e.g., [Balenzano et al., 2021](#); [Balenzano et al., 2012](#); [De Zan & Gomba, 2018](#); [De Zan et al., 2014](#); [Nolan & Fatland, 2003](#); [Zwieback et al., 2015](#)). A recent study seems to demonstrate the same relationship over peatlands with Sentinel-1 C-band phase because of intense and fast soil moisture changes ([Hrysiewicz et al., 2023](#)). According to the current models of the soil-moisture/InSAR-phase relationships, soil moisture changes should cause underestimations of InSAR displacements, decreasing the amplitudes of observed vertical displacements and the InSAR coherence ([De Zan & Gomba, 2018](#); [De Zan et al., 2014](#)).

On peatlands, the resulting challenges may be resumed as our ability to separate the soil-moisture-related phases, the deviations due to phase ambiguities and phase biases. For example, this can be done using SAR data with larger wavelength such as L- and S-band sensors. Indeed L-band InSAR should not be subjected to phase ambiguity because the maximal displacements are lower than the quarter of L-band wavelength ( $\lambda = 30$  cm) and can maximise the InSAR coherence. However, this

should lead to an increase of potential deviations (in terms of displacements) due to soil moisture changes because the wavelength is larger in L-band. Further studies should therefore examine these deviations using Sentinel-1 C-band data associated with L band (or perhaps S band) and *in-situ* measurements, (with long-term periods of observation), giving the new SAR/InSAR mission NISAR as an expected suitable tool, associated with C-band Sentinel-1 imagery, for peat-ground-surface monitoring (N.B.: NISAR, launched in 2024, will operate in L and S bands, with a 12-day temporal resolution).

### **5.5. Transferability to other peatlands**

In terms of transferability of this method to other peatlands (for example upland blanket bogs and lowland fens), we must consider two challenges:

1. The temporal oscillating InSAR coherence. This allows us to produce interferogram networks by using long-term interferograms – potentially not observable on other peatlands which can be destroyed by human activities in other European countries (e.g., harvested bogs). From our experiences, InSAR seems to work on intact bogs but it is difficult to obtain acceptable InSAR coherence with long-term interferometric pairs, on highly degraded bogs, afforested bogs, or bogs with bare peat. These ability to maintain InSAR coherence could be dependent on the hydrological function of the degraded system. In addition, peatlands in boreal or continental climates may be more difficult targets because of annual periods of snow/ice cover, destroying InSAR coherence;
2. the ability to have interferograms without phase ambiguity. For Cors Fochno and Cors Caron, the amplitude of annual displacement oscillations is relatively low compared to some boreal peatlands ([Tampuu et al., 2022](#)). The use of 2-conn. or 1-conn. (i.e., daisy chain) networks should be investigated, along with the use of higher wavelength (e.g., L-band SAR sensor) in

order to capture the complete amplitude of displacement oscillations. Work in the Netherlands by [Conroy et al. \(2022\)](#) also proposes to use a subset of ground observation data to resolve the phase ambiguity issue.

## 5.6. InSAR-derived displacements as a proxy for groundwater levels

Recent works have shown linkages between InSAR displacements of peatland and groundwater levels in terms of the main control on the seasonal oscillation of the peat surface ([Alshammari et al., 2020](#); [Hrysiewicz et al., 2023](#)). In our study, we also provide such links but over longer time series, and with a closer approximation – ground-validated by *in-situ* displacement measurements – of the surface oscillation related to groundwater level oscillation. These displacements are synchronous with our observations of groundwater levels with a conversion factor of  $\sim 1:10$  ( $R_{ad}^2 = 0.45$ ) for Cors Fochno and  $\sim 1:20$  ( $R_{ad}^2 = 0.36$ ) for Cors Caron (see **Figure 11** and **Figure 12**). However, the factor estimated for Cors Caron could be underestimated because of the lack of groundwater-level measurements for much of the observation period. The durations of InSAR time series (and groundwater-level measurements) allow us to demonstrate that the peat surface motions lag the water table by several days/weeks. In addition, **Figure 12a** shows that the relationships between long-term groundwater-level change rates and displacement rates are not clear.

Furthermore, our study provides a first link between the peat thickness, the peat elevation and the long-term displacement rate derived from InSAR. Long-term displacement rates also negatively correlate with both dome elevation, especially on Cors Fochno, and peat thicknesses (see **Figure 15a** and **Figure 15b**), with linear relationships ranging from  $-3 \text{ mm}\cdot\text{yr}^{-1}\cdot\text{m}^{-1}$  to  $-0.5 \text{ mm}\cdot\text{yr}^{-1}\cdot\text{m}^{-1}$ . Such relation has also been seen via previous studies using differencing of elevation maps made by *in-situ* and LiDAR measurements at another raised bog (Clara bog, Co. Offaly, Ireland) ([Regan et al., 2019](#)).

This relationship can be consistent with the elevation decrease on Cors Fochno, between 2009 and

2020-2022 (see **Figure 14**). This relationship could be an indirect access to the hydrological system and the geomorphological features of bogs ([Cobb et al., 2017](#)).

These observations reflect an overriding control on the long-term peat surface motion from compaction of the full peat column: i.e., a deeper-seated driving mechanism than that driving the seasonal oscillations. This could provide information on the peat mechanical parameters (density, elastic modulus, etc.). Nevertheless, further studies, with monitoring of deep water levels and more robust estimation of displacement/thickness relationships, are required to support this interpretation.

## 6. Conclusion

By using a combination of long and short temporal baseline networks, the InSAR method can be used to estimate peat ground surface displacements from Sentinel-1 C-band IW data. (see upper part of **Figure 16**). We demonstrate that InSAR estimates of peat surface displacements are valid compared to sub-millimetric data from in-situ measurements of displacements via “peat cameras”. We show that InSAR estimates can capture the features of peat surface oscillations (“bog breathing”) with high-accuracy estimation. The long-term displacement rates of peat surface motion are not currently well validated with the same robustness as short-term displacements because of the relative short *in-situ* time series and the non-steady amplitude of seasonal oscillations.

Regarding the linkages between displacement and groundwater levels, we have shown that annual oscillations are directly related to groundwater levels with a ratio from 1:20 to 1:10. Long-term peat displacement rates are not correlated to those of average long-term groundwater level in the study sites. Instead, the long-term displacement rates are correlated with dome elevation and peat thickness. Furthermore, these correlations are complicated by time lags between groundwater movements and peat surface response.

This manuscript is a non-peer reviewed preprint and has been submitted for publication in Remote Sensing of Environment. Please note that subsequent versions of this manuscript may have different content. Please feel free to contact any of the authors; we welcome feedback.

Overall, InSAR methods seem ready to monitor the surface displacements of temperate raised bogs and to map remotely the peat ecohydrological parameters, at large scale, high spatial resolution, and low-cost. For example, InSAR-derived displacements can be an efficient proxy of short-term groundwater level changes: key parameter of peatlands in order to estimate the GHG emissions.

## **Data availability**

The additional figures can be found in the Supplementary Materials. All the InSAR products and scripts used to analyse the observations are available from the corresponding author.

## **CRedit authorship contribution statement**

**Alexis Hrysiewicz:** Conceptualisation, Data computation, Investigation and Analysis, Methodology, Visualisation, Writing – original draft. **Jennifer Williamson:** In-situ data extraction and Investigation, Writing – original draft. **Chris Evans:** Conceptualisation, Methodology, Writing – original draft. **A. Jonay Jovani-Sancho:** In-situ methodology and Data Investigation. **Nathan Callaghan:** In-situ methodology and data extraction. **Justin Lyons:** Investigation and Analysis, In-situ data extraction and Investigation, Writing – original draft. **Jake White:** Investigation and Analysis, In-situ data extraction and Investigation. **Joanna Kowalska:** In-situ data extraction. **Nina Menichino:** Writing – original draft. **Eoghan Holohan:** Supervision, Project Funding and administration, Conceptualisation, Investigation and Analysis, Methodology, Visualisation, Writing – original draft.

## Acknowledgments

The authors thank past and present members of the iCrag senior research management team and operations team for their support of the InSAR lab and our related peatlands research at UCD. We also thank the staff of GAMMA Remote Sensing AG for training and technical support. We thank NRW staff members Jack Simpson, Rhoswen Leonard, Fleur Miles-Farrier, Ben Soanes, Rebecca Thomas, Osian Fudge, Dan Hersee, & Jon Walker for retrieving the peat height camera data from the field. We acknowledge the European Space Agency (ESA) for the Sentinel-1 data, NASA for SRTM DEM and the Wales government for the availability of the 2020-2022 Lidar DSM (under Open Government License: <https://www.nationalarchives.gov.uk/doc/open-government-licence/version/3/>). We also thank (Wessel et al., 2019) for the development and availability of GMT6. The authors acknowledge funding from iCrag, the Science Foundation Ireland Research Centre in Applied Geosciences (iCrag-Phase 2 – Grand Code: 13/RC/2092\_P2) to EPH, and an ESA Living Planet Fellowship to AH (Grand Code: 73738). NRW acknowledges funding from the EU LIFE programme for restoration and monitoring work under the “LIFE Welsh Raised Bogs project” (Grant code: LIFE16 NAT/UK/000646).

## Declaration of Competing Interest

The authors declare no competing interests.

## References

- Alshammari, L., Boyd, D. S., Sowter, A., Marshall, C., Andersen, R., Gilbert, P., Marsh, S., & Large, D. J. (2020). Use of Surface Motion Characteristics Determined by InSAR to Assess Peatland Condition. *Journal of Geophysical Research: Biogeosciences*, 125(1). <https://doi.org/10.1029/2018jg004953>

- Alshammari, L., Large, D. J., Boyd, D. S., Sowter, A., Anderson, R., Andersen, R., & Marsh, S. (2018). Long-Term Peatland Condition Assessment via Surface Motion Monitoring Using the ISBAS DInSAR Technique over the Flow Country, Scotland. *Remote Sensing*, 10(7).
- Amidror, I. (2002). Scattered data interpolation methods for electronic imaging systems: a survey. *Journal of Electronic Imaging*, 11(2), 157-176. <https://doi.org/10.1117/1.1455013>
- Ansari, H., De Zan, F., & Parizzi, A. (2021). Study of Systematic Bias in Measuring Surface Deformation With SAR Interferometry. *IEEE Transactions on Geoscience and Remote Sensing*, 59(2), 1285-1301. <https://doi.org/https://doi.org/10.1109/TGRS.2020.3003421>
- Asmuß, T., Bechtold, M., & Tiemeyer, B. (2018). Towards monitoring groundwater table depth in peatlands from Sentinel-1 radar data. IGARSS 2018-2018 IEEE International Geoscience and Remote Sensing Symposium,
- Balenzano, A., Mattia, F., Satalino, G., Lovergine, F. P., Palmisano, D., Peng, J., Marzahn, P., Wegmüller, U., Cartus, O., Dąbrowska-Zielińska, K., Musial, J. P., Davidson, M. W. J., Pauwels, V. R. N., Cosh, M. H., McNairn, H., Johnson, J. T., Walker, J. P., Yueh, S. H., Entekhabi, D., . . . Jackson, T. J. (2021). Sentinel-1 soil moisture at 1 km resolution: a validation study. *Remote Sensing of Environment*, 263. <https://doi.org/10.1016/j.rse.2021.112554>
- Balenzano, A., Mattia, F., Satalino, G., Pauwels, V., & Snoeij, P. (2012). SMOSAR algorithm for soil moisture retrieval using Sentinel-1 data. 2012 IEEE International Geoscience and Remote Sensing Symposium,
- Bechtold, M., Schlaffer, S., Tiemeyer, B., & De Lannoy, G. (2018). Inferring Water Table Depth Dynamics from ENVISAT-ASAR C-Band Backscatter over a Range of Peatlands from Deeply-Drained to Natural Conditions. *Remote Sensing*, 10(4). <https://doi.org/10.3390/rs10040536>
- Biggs, J., & Pritchard, M. E. (2017). Global Volcano Monitoring: What Does It Mean When Volcanoes Deform? *Elements*, 13(1), 17-22. <https://doi.org/https://doi.org/10.2113/gselements.13.1.17>
- Boncori, J. P. M. (2019). Measuring Coseismic Deformation With Spaceborne Synthetic Aperture Radar: A Review. *Frontiers in Earth Science*, 7. <https://doi.org/https://doi.org/10.3389/feart.2019.00016>
- Bradley, A. V., Andersen, R., Marshall, C., Sowter, A., & Large, D. J. (2022). Identification of typical ecohydrological behaviours using InSAR allows landscape-scale mapping of peatland condition. *Earth Surface Dynamics*, 10(2), 261-277. <https://doi.org/10.5194/esurf-10-261-2022>
- Burgmann, R., Rosen, P. A., & Fielding, E. J. (2000). Synthetic aperture radar interferometry to measure Earth's surface topography and its deformation. *Annual Review of Earth and Planetary Sciences*, 28, 169-209. <https://doi.org/DOI 10.1146/annurev.earth.28.1.169>
- Casu, F., Manzo, M., & Lanari, R. (2006). A quantitative assessment of the SBAS algorithm performance for surface deformation retrieval from DInSAR data. *Remote Sensing of Environment*, 102(3-4), 195-210. <https://doi.org/https://doi.org/10.1016/j.rse.2006.01.023>
- Chen, C. W., & Zebker, H. A. (2000). Network approaches to two-dimensional phase unwrapping: intractability and two new algorithms. *Journal of the Optical Society of America A*, 17(3), 401-414. <https://doi.org/10.1364/JOSAA.17.000401>
- Chen, C. W., & Zebker, H. A. (2001). Two-dimensional phase unwrapping with use of statistical models for cost functions in nonlinear optimization. *Journal of the Optical Society of America A*, 18(2), 338-351. <https://doi.org/10.1364/JOSAA.18.000338>

- Chen, C. W., & Zebker, H. A. (2002). Phase unwrapping for large SAR interferograms: statistical segmentation and generalized network models. *IEEE Transactions on Geoscience and Remote Sensing*, 40(8), 1709-1719. <https://doi.org/10.1109/TGRS.2002.802453>
- Cobb, A. R., Hoyt, A. M., Gandois, L., Eri, J., Dommmain, R., Abu Salim, K., Kai, F. M., Haji Su'ut, N. S., & Harvey, C. F. (2017). How temporal patterns in rainfall determine the geomorphology and carbon fluxes of tropical peatlands. *Proceedings of the National Academy of Sciences*, 114(26), E5187-E5196. <https://doi.org/doi:10.1073/pnas.1701090114>
- Connolly, J., & Holden, N. M. (2009). Mapping peat soils in Ireland: updating the derived Irish peat map. *Irish Geography*, 42(3), 343-352. <https://doi.org/10.1080/00750770903407989>
- Connolly, J., & Holden, N. M. (2017). Detecting peatland drains with Object Based Image Analysis and Geosy-1 imagery. *Carbon Balance and Management*, 12(1). <https://doi.org/10.1186/s13021-017-0075-z>
- Conroy, P., Diepen, S. A. N. v., Asselen, S. V., Erkens, G., Leijen, F. J. v., & Hanssen, R. F. (2022). Probabilistic Estimation of InSAR Displacement Phase Guided by Contextual Information and Artificial Intelligence. *IEEE Transactions on Geoscience and Remote Sensing*, 60, 1-11. <https://doi.org/10.1109/TGRS.2022.3203872>
- De Luca, C., Casu, F., Manunta, M., Onorato, G., & Lanari, R. (2022). Comments on “Study of Systematic Bias in Measuring Surface Deformation With SAR Interferometry”. *IEEE Transactions on Geoscience and Remote Sensing*, 60, 1-5. <https://doi.org/10.1109/tgrs.2021.3103037>
- De Zan, F., & Gomba, G. (2018). Vegetation and soil moisture inversion from SAR closure phases: First experiments and results. *Remote Sensing of Environment*, 217, 562-572. <https://doi.org/10.1016/j.rse.2018.08.034>
- De Zan, F., Parizzi, A., Prats-Iraola, P., & López-Dekker, P. (2014). A SAR interferometric model for soil moisture. *IEEE Transactions on Geoscience and Remote Sensing*, 52(1), 418-425. <https://doi.org/10.1109/TGRS.2013.2241069>
- De Zan, F., Zonno, M., & Lopez-Dekker, P. (2015). Phase Inconsistencies and Multiple Scattering in SAR Interferometry. *IEEE Transactions on Geoscience and Remote Sensing*, 53(12), 6608-6616. <https://doi.org/10.1109/tgrs.2015.2444431>
- Drösler, M., Freibauer, A., Torben, C. R., & Friborg, T. (2008). Observations and status of peatland greenhouse gas emissions in Europe. In *The Continental-Scale Greenhouse Gas Balance of Europe* (pp. 243--261). Springer. <https://doi.org/10.1007/978-0-387-76570-9>
- Evans, C. D., Artz, R., Moxley, J., Smyth, E. T., Taylor, E., Archer, N., Burden, A., Williamson, J., Donnelly, D., Thomson, A., Buys, G., Renou-Wilson, F., & Potts, J. (2017). *Implementation of an emissions inventory for UK peatlands (updated)*.
- Evans, C. D., Callaghan, N., Jaya, A., Grinham, A., Sjogersten, S., Page, S. E., Harrison, M. E., Kusin, K., Kho, L. K., Ledger, M., Evers, S., Mitchell, Z., Williamson, J., Radbourne, A. D., & Jovani-Sancho, A. J. (2021). A Novel Low-Cost, High-Resolution Camera System for Measuring Peat Subsidence and Water Table Dynamics. *Frontiers in Environmental Science*, 9. <https://doi.org/10.3389/fenvs.2021.630752>
- Evans, C. D., Peacock, M., Baird, A. J., Artz, R. R. E., Burden, A., Callaghan, N., Chapman, P. J., Cooper, H. M., Coyle, M., Craig, E., Cumming, A., Dixon, S., Gauci, V., Grayson, R. P., Helfter, C., Heppell, C. M., Holden, J., Jones, D. L., Kaduk, J., . . . Morrison, R. (2021). Overriding water table control on managed peatland greenhouse gas emissions. *Nature*, 593(7860), 548-552. <https://doi.org/10.1038/s41586-021-03523-1>
- Evans, C. D., Williamson, J. M., Kacaribu, F., Irawan, D., Suardiwerianto, Y., Hidayat, M. F., Laurén, A., & Page, S. E. (2019). Rates and spatial variability of peat subsidence in Acacia plantation

- and forest landscapes in Sumatra, Indonesia. *Geoderma*, 338, 410-421. <https://doi.org/10.1016/j.geoderma.2018.12.028>
- Farr, T. G., Rosen, P. A., Caro, E., Crippen, R., Duren, R., Hensley, S., Kobrick, M., Paller, M., Rodriguez, E., Roth, L., Seal, D., Shaffer, S., Shimada, J., Umland, J., Werner, M., Oskin, M., Burbank, D., & Alsdorf, D. (2007). The shuttle radar topography mission. *Reviews of Geophysics*, 45(2). <https://doi.org/https://doi.org/10.1029/2005RG000183>
- Ferretti, A., Fumagalli, A., Novali, F., Prati, C., Rocca, F., & Rucci, A. (2011). A New Algorithm for Processing Interferometric Data-Stacks: SqueeSAR. *IEEE Transactions on Geoscience and Remote Sensing*, 49(9), 3460-3470. <https://doi.org/https://doi.org/10.1109/TGRS.2011.2124465>
- Ferretti, A., Prati, C., & Rocca, F. (2001). Permanent scatterers in SAR interferometry. *IEEE Transactions on Geoscience and Remote Sensing*, 39(1), 8-20. <https://doi.org/https://doi.org/10.1109/36.898661>
- Ferretti, A., Savio, G., Barzaghi, R., Borghi, A., Musazzi, S., Novali, F., Prati, C., & Rocca, F. (2007). Submillimeter Accuracy of InSAR Time Series: Experimental Validation. *IEEE Transactions on Geoscience and Remote Sensing*, 45(5), 1142-1153. <https://doi.org/10.1109/TGRS.2007.894440>
- Fiaschi, S., Holohan, E. P., Sheehy, M., & Floris, M. (2019). PS-InSAR Analysis of Sentinel-1 Data for Detecting Ground Motion in Temperate Oceanic Climate Zones: A Case Study in the Republic of Ireland. *Remote Sensing*, 11(3). <https://doi.org/10.3390/rs11030348>
- Fritsch, F. N., & Carlson, R. E. (1980). Monotone Piecewise Cubic Interpolation. *SIAM Journal on Numerical Analysis*, 17(2), 238-246. <https://doi.org/Doi 10.1137/0717021>
- Godwin, H. (1943). Coastal Peat Beds of the British Isles and North Sea: Presidential Address to the British Ecological Society 1943. *Journal of Ecology*, 31(2), 199-247. <https://doi.org/10.2307/2256548>
- Gorham, E. (1991). Northern Peatlands: Role in the Carbon Cycle and Probable Responses to Climatic Warming. *Ecol Appl*, 1(2), 182-195. <https://doi.org/10.2307/1941811>
- Hanssen, R. F. (2001). *Radar interferometry: data interpretation and error analysis* (Vol. 2). Springer Science & Business Media.
- Hiraishi, T., Krug, T., Tanabe, K., Srivastava, N., Baasansuren, J., Fukuda, M., & Troxler, T. (2014). 2013 supplement to the 2006 IPCC guidelines for national greenhouse gas inventories: Wetlands. *IPCC, Switzerland*.
- Hollis, D., McCarthy, M., Kendon, M., Legg, T., & Simpson, I. (2019). HadUK-Grid-A new UK dataset of gridded climate observations. *Geoscience Data Journal*, 6(2), 151-159. <https://doi.org/10.1002/gdj3.78>
- Hooijer, A., Page, S., Canadell, J. G., Silvius, M., Kwadijk, J., Wösten, H., & Jauhiainen, J. (2010). Current and future CO<sub>2</sub> emissions from drained peatlands in Southeast Asia. *Biogeosciences*, 7(5), 1505-1514. <https://doi.org/10.5194/bg-7-1505-2010>
- Hooijer, A., Page, S., Jauhiainen, J., Lee, W. A., Lu, X. X., Idris, A., & Anshari, G. (2012). Subsidence and carbon loss in drained tropical peatlands. *Biogeosciences*, 9(3), 1053-1071. <https://doi.org/10.5194/bg-9-1053-2012>
- Hooijer, A., Page, S., Navratil, P., Vernimmen, R., & Mawdsley, N. (2014). Carbon Emissions from Drained and Degraded Peatland in Indonesia and Emission Factors for Measurement, Reporting and Verification (MRV) of Peatland Greenhouse Gas Emissions. *Fordamof.org*(May), 50-50.
- Hooper, A. (2008). A multi-temporal InSAR method incorporating both persistent scatterer and small baseline approaches. *Geophysical Research Letters*, 35(16). <https://doi.org/https://doi.org/10.1029/2008GL034654>

- Hooper, A., Bekaert, D., Spaans, K., & Arikan, M. (2012). Recent advances in SAR interferometry time series analysis for measuring crustal deformation. *Tectonophysics*, 514, 1-13. <https://doi.org/https://doi.org/10.1016/j.tecto.2011.10.013>
- Hooper, A., & Zebker, H. A. (2007). Phase unwrapping in three dimensions with application to InSAR time series. *Journal of the Optical Society of America A*, 24(9), 2737-2747. <https://doi.org/10.1364/JOSAA.24.002737>
- Howie, S. A., & Hebda, R. J. (2018). Bog surface oscillation (mire breathing): A useful measure in raised bog restoration. *Hydrological Processes*, 32(11), 1518-1530. <https://doi.org/10.1002/hyp.11622>
- Hoyt, A. M., Chaussard, E., Seppäläinen, S. S., & Harvey, C. F. (2020). Widespread subsidence and carbon emissions across Southeast Asian peatlands. *Nature Geoscience*, 13(6), 435-440. <https://doi.org/10.1038/s41561-020-0575-4>
- Hrysiewicz, A., Holohan, E. P., Donohue, S., & Cushnan, H. (2023). SAR and InSAR data linked to soil moisture changes on a temperate raised peatland subjected to a wildfire. *Remote Sensing of Environment*, 291. <https://doi.org/10.1016/j.rse.2023.113516>
- Joosten, H., Sirin, A., Couwenberg, J., Laine, J., & Smith, P. (2016). The role of peatlands in climate regulation. In A. Bonn, H. Joosten, M. Evans, R. Stoneman, & T. Allott (Eds.), *Peatland Restoration and Ecosystem Services: Science, Policy and Practice* (pp. 63-76). Cambridge University Press. <https://doi.org/DOI:10.1017/CBO9781139177788.005>
- Kahaner, D., Moler, C., & Nash, S. (1989). *Numerical methods and software*. Prentice-Hall, Inc.
- Kim, J.-W., Lu, Z., Gutenberg, L., & Zhu, Z. (2017). Characterizing hydrologic changes of the Great Dismal Swamp using SAR/InSAR. *Remote Sensing of Environment*, 198, 187-202. <https://doi.org/10.1016/j.rse.2017.06.009>
- Köchy, M., Hiederer, R., & Freibauer, A. (2015). Global distribution of soil organic carbon – Part 1: Masses and frequency distributions of SOC stocks for the tropics, permafrost regions, wetlands, and the world. *Soil*, 1(1), 351-365. <https://doi.org/10.5194/soil-1-351-2015>
- Lees, K. J., Quaife, T., Artz, R. R. E., Khomik, M., & Clark, J. M. (2018). Potential for using remote sensing to estimate carbon fluxes across northern peatlands – A review. *Science of the Total Environment*, 615, 857-874. <https://doi.org/10.1016/j.scitotenv.2017.09.103>
- Leifeld, J., & Menichetti, L. (2018). The underappreciated potential of peatlands in global climate change mitigation strategies. *Nature Communications*, 9.
- Letts, M. G., Roulet, N. T., Comer, N. T., Skarupa, M. R., & Verseghy, D. L. (2000). Parametrization of peatland hydraulic properties for the Canadian Land Surface Scheme. *Atmosphere-Ocean*, 38(1), 141-160. <https://doi.org/Doi10.1080/07055900.2000.9649643>
- Marshall, C., Sterk, H. P., Gilbert, P. J., Andersen, R., Bradley, A. V., Sowter, A., Marsh, S., & Large, D. J. (2022). Multiscale Variability and the Comparison of Ground and Satellite Radar Based Measures of Peatland Surface Motion for Peatland Monitoring. *Remote Sensing*, 14(2). <https://doi.org/10.3390/rs14020336>
- Massonnet, D., & Feigl, K. L. (1998). Radar interferometry and its application to changes in the earth's surface. *Reviews of Geophysics*, 36(4), 441-500. <https://doi.org/10.1029/97RG03139>
- Millard, K., & Richardson, M. (2018). Quantifying the relative contributions of vegetation and soil moisture conditions to polarimetric C-Band SAR response in a temperate peatland. *Remote Sensing of Environment*, 206, 123-138. <https://doi.org/10.1016/j.rse.2017.12.011>
- Millard, K., Thompson, D. K., Parisien, M. A., & Richardson, M. (2018). Soil moisture monitoring in a temperate peatland using multi-sensor remote sensing and linear mixed effects. *Remote Sensing*, 10(6). <https://doi.org/10.3390/rs10060903>

- Molan, Y. E., Lu, Z., & Kim, J.-W. (2020). Influence of the Statistical Properties of Phase and Intensity on Closure Phase. *IEEE Transactions on Geoscience and Remote Sensing*, 58(10), 7346-7354. <https://doi.org/10.1109/tgrs.2020.2982062>
- Morton, P. A., & Heinemeyer, A. (2019). Bog breathing: the extent of peat shrinkage and expansion on blanket bogs in relation to water table, heather management and dominant vegetation and its implications for carbon stock assessments. *Wetlands Ecology and Management*, 27(4), 467-482. <https://doi.org/10.1007/s11273-019-09672-5>
- Nolan, M., & Fatland, D. R. (2003). Penetration depth as a DInSAR observable and proxy for soil moisture. *IEEE Transactions on Geoscience and Remote Sensing*, 41(3), 532-537. <https://doi.org/10.1109/tgrs.2003.809931>
- Osmanoğlu, B., Sunar, F., Wdowinski, S., & Cabral-Cano, E. (2016). Time series analysis of InSAR data: Methods and trends. *Isprs Journal of Photogrammetry and Remote Sensing*, 115, 90-102. <https://doi.org/https://doi.org/10.1016/j.isprsjprs.2015.10.003>
- Paloscia, S., Pettinato, S., Santi, E., Notarnicola, C., Pasolli, L., & Reppucci, A. (2013). Soil moisture mapping using Sentinel-1 images: Algorithm and preliminary validation. *Remote Sensing of Environment*, 134, 234-248. <https://doi.org/10.1016/j.rse.2013.02.027>
- Peng, J., Albergel, C., Balenzano, A., Brocca, L., Cartus, O., Cosh, M. H., Crow, W. T., Dabrowska-Zielinska, K., Dadson, S., Davidson, M. W. J., de Rosnay, P., Dorigo, W., Gruber, A., Hagemann, S., Hirschi, M., Kerr, Y. H., Lovergine, F., Mahecha, M. D., Marzahn, P., . . . Loew, A. (2021). A roadmap for high-resolution satellite soil moisture applications – confronting product characteristics with user requirements. *Remote Sensing of Environment*, 252. <https://doi.org/10.1016/j.rse.2020.112162>
- Pinel, V., Poland, M. P., & Hooper, A. (2014). Volcanology: Lessons learned from Synthetic Aperture Radar imagery. *Journal of Volcanology and Geothermal Research*, 289, 81-113. <https://doi.org/https://doi.org/10.1016/j.jvolgeores.2014.10.010>
- Reeve, A. S., Glaser, P. H., & Rosenberry, D. O. (2013). Seasonal changes in peatland surface elevation recorded at GPS stations in the Red Lake Peatlands, northern Minnesota, USA. *Journal of Geophysical Research-Biogeosciences*, 118(4), 1616-1626. <https://doi.org/10.1002/2013jg002404>
- Regan, S., Flynn, R., Gill, L., Naughton, O., & Johnston, P. (2019). Impacts of Groundwater Drainage on Peatland Subsidence and Its Ecological Implications on an Atlantic Raised Bog. *Water Resources Research*, 55(7), 6153-6168. <https://doi.org/10.1029/2019wr024937>
- Renou-Wilson, F., Moser, G., Fallon, D., Farrell, C. A., Müller, C., & Wilson, D. (2019). Rewetting degraded peatlands for climate and biodiversity benefits: Results from two raised bogs. *Ecological Engineering*, 127, 547-560. <https://doi.org/10.1016/j.ecoleng.2018.02.014>
- Sansosti, E., Berardino, P., Bonano, M., Calò, F., Castaldo, R., Casu, F., Manunta, M., Manz, M., Pepe, A., Pepe, S., Solaro, G., Tizzani, P., Zeni, G., & Lanari, R. (2014). How second generation SAR systems are impacting the analysis of ground deformation. *International Journal of Applied Earth Observation and Geoinformation*, 28, 1-11. <https://doi.org/https://doi.org/10.1016/j.jag.2013.10.007>
- Smith, P., Bustamante, M., Ahammad, H., Clark, H., Dong, H., Elsiddig, E. A., Haberl, H., Harper, R., House, J., & Jafari, M. (2014). Agriculture, forestry and other land use (AFOLU). In *Climate change 2014: mitigation of climate change. Contribution of Working Group III to the Fifth Assessment Report of the Intergovernmental Panel on Climate Change* (pp. 811-922). Cambridge University Press.
- Smyth, E. T., Archer, N., Burden, A., Williamson, J., Donnelly, D., Thomson, A., Buys, G., Malcolm, H., Wilson, D., & Renou-Wilson, F. (2017). *Implementation of an emissions inventory for UK peatlands*.

- Takada, M., Mishima, Y., & Natsume, S. (2009). Estimation of surface soil properties in peatland using ALOS/PALSAR. *Landscape and Ecological Engineering*, 5(1), 45-58. <https://doi.org/10.1007/s11355-008-0061-4>
- Tampuu, T. (2022). *Synthetic Aperture Radar Interferometry as a tool for monitoring the dynamics of peatland surface* University of Tartu].
- Tampuu, T., De Zan, F., Shau, R., Praks, J., Kohv, M., & Kull, A. (2022). CAN Bog Breathing be Measured by Synthetic Aperture Radar Interferometry. IGARSS 2022-2022 IEEE International Geoscience and Remote Sensing Symposium,
- Thollard, F., Clesse, D., Doin, M. P., Donadieu, J., Durand, P., Grandin, R., Lasserre, C., Laurent, C., Deschamps-Ostanciaux, E., Pathier, E., Pointal, E., Proy, C., & Specht, B. (2021). FLATSIM: The ForM@Ter LArge-Scale Multi-Temporal Sentinel-1 InterferoMetry Service. *Remote Sensing*, 13(18). <https://doi.org/https://doi.org/10.3390/rs13183734>
- Van den Akker, J., Jansen, P., Hendriks, R., Hoving, I., & Pleijter, M. (2012). Submerged infiltration to halve subsidence and GHG emissions of agricultural peat soils. Proceedings of the 14th International Peat Congress, Stockholm, Sweden,
- Wagner, W., Sabel, D., Doubkova, M., Bartsch, A., & Pathe, C. (2013). the Potential of Sentinel-1 for Monitoring Soil Moisture With a High Spatial Resolution At Global Scale. *Cycle*, 2009(November 2009), 18-20.
- Wegmüller, U., Werner, C., Strozzi, T., & Wiesmann, A. (2004). Multi-temporal interferometric point target analysis. In *Analysis of multi-temporal remote sensing images* (pp. 136-144). World Scientific.
- Wegmüller, U., Werner, C., Strozzi, T., Wiesmann, A., Frey, O., & Santoro, M. (2015). Sentinel-1 IWS mode support in the GAMMA software. 2015 IEEE 5th Asia-Pacific Conference on Synthetic Aperture Radar (APSAR),
- Werner, C., Wegmuller, U., Strozzi, T., & Wiesmann, A. (2003, 21-25 July 2003). Interferometric point target analysis for deformation mapping. IGARSS 2003. 2003 IEEE International Geoscience and Remote Sensing Symposium. Proceedings (IEEE Cat. No.03CH37477),
- Wessel, P., Luis, J. F., Uieda, L., Scharroo, R., Wobbe, F., Smith, W. H. F., & Tian, D. (2019). The Generic Mapping Tools Version 6. *Geochemistry, Geophysics, Geosystems*, 20(11), 5556-5564. <https://doi.org/10.1029/2019gc008515>
- Wright, T. J. (2004). Toward mapping surface deformation in three dimensions using InSAR. *Geophysical Research Letters*, 31(1). <https://doi.org/10.1029/2003gl018827>
- Xu, J., Morris, P. J., Liu, J., & Holden, J. (2018). PEATMAP: Refining estimates of global peatland distribution based on a meta-analysis. *Catena*, 160, 134-140.
- Yu, Z., Loisel, J., Brosseau, D. P., Beilman, D. W., & Hunt, S. J. (2010). Global peatland dynamics since the Last Glacial Maximum. *Geophysical Research Letters*, 37(13), n/a-n/a. <https://doi.org/10.1029/2010gl043584>
- Zebker, H. A., & Villasenor, J. (1992). Decorrelation in Interferometric Radar Echoes. *IEEE Transactions on Geoscience and Remote Sensing*, 30(5), 950-959. <https://doi.org/https://doi.org/10.1109/36.175330>
- Zheng, Y., Fattahi, H., Agram, P., Simons, M., & Rosen, P. (2022). On Closure Phase and Systematic Bias in Multilooked SAR Interferometry. *IEEE Transactions on Geoscience and Remote Sensing*, 60, 1-11. <https://doi.org/10.1109/tgrs.2022.3167648>
- Zhou, Z. (2013). *The applications of InSAR time series analysis for monitoring long-term surface change in peatlands* University of Glasgow].
- Zhou, Z. W., Li, Z. H., Waldron, S., & Tanaka, A. (2016). Monitoring Peat Subsidence and Carbon Emission in Indonesia Peatlands Using Insar Time Series. *2016 Ieee International Geoscience*

This manuscript is a non-peer reviewed preprint and has been submitted for publication in Remote Sensing of Environment. Please note that subsequent versions of this manuscript may have different content. Please feel free to contact any of the authors; we welcome feedback.

*and Remote Sensing Symposium (Igarss), 6797-6798.*  
<https://doi.org/10.1109/Igarss.2016.7730774>

Zwieback, S., Hensley, S., & Hajnsek, I. (2015). Assessment of soil moisture effects on L-band radar interferometry. *Remote Sensing of Environment, 164, 77-89.*  
<https://doi.org/10.1016/j.rse.2015.04.012>

Zwieback, S., Hensley, S., & Hajnsek, I. (2017). Soil Moisture Estimation Using Differential Radar Interferometry: Toward Separating Soil Moisture and Displacements. *IEEE Transactions on Geoscience and Remote Sensing, 55(9), 5069-5083.*  
<https://doi.org/10.1109/tgrs.2017.2702099>